Perturbation Theory for BAO reconstructed fields: one-loop results in real-space matter density field

Chiaki Hikage

Kavli Institute for the Physics and Mathematics of the Universe (Kavli IPMU, WPI), University of Tokyo, 5-1-5 Kashiwanoha, Kashiwa, Chiba, 277-8583, Japan *

Kazuya Koyama

Institute of Cosmology and Gravitation, University of Portsmouth, Portsmouth PO1 3FX, UK

Alan Heavens

Imperial Centre for Inference and Cosmology (ICIC), Department of Physics, Imperial College London, Blackett Laboratory, Prince Consort Road, London SW7 2AZ, UK

(Dated: July 25, 2017)

We compute the power spectrum at one loop order in standard perturbation theory for the matter density field to which a standard Lagrangian Baryonic acoustic oscillation (BAO) reconstruction technique is applied. The BAO reconstruction method corrects the bulk motion associated with the gravitational evolution using the inverse Zel'dovich approximation (ZA) for the smoothed density field. We find that the overall amplitude of one-loop contributions in the matter power spectrum substantially decrease after reconstruction. The reconstructed power spectrum thereby approaches the initial linear spectrum when the smoothed density field is close enough to linear, i.e., the smoothing scale $R_s \gtrsim 10 h^{-1}$Mpc. On smaller R_s, however, the deviation from the linear spectrum becomes significant on large scales ($k \lesssim R_s^{-1}$) due to the nonlinearity in the smoothed density field, and the reconstruction is inaccurate. Compared with N-body simulations, we show that the reconstructed power spectrum at one loop order agrees with simulations better than the unreconstructed power spectrum. We also calculate the tree-level bispectrum in standard perturbation theory to investigate non-Gaussianity in the reconstructed matter density field. We show that the amplitude of the bispectrum significantly decreases for small k after reconstruction and that the tree-level bispectrum agrees well with N-body results in the weakly nonlinear regime.

I. INTRODUCTION

Large-scale structure in our Universe has been widely used for a variety of cosmological studies. The Baryonic Acoustic Oscillation (BAO) signature imprinted in the large-scale structure plays a role as a standard ruler to probe the expansion history of the Universe or dark energy [e.g., 1]. BAOs have been detected in various galaxy surveys and used for cosmological studies [e.g., 2–6]. The broad shape of the power spectrum of evolved density fluctuations provides a cosmological probe complementary to the Cosmic Microwave Background [3, 5, 7, 8] and a probe of massive neutrinos [e.g., 9, 10]. Both the power spectrum and the bispectrum are also sensitive to the primordial non-Gaussianity [e.g., 11–14].

Nonlinear growth of cosmic large-scale structure and the resulting bulk flow motion degrade the BAO signals and also biases the measurements of BAO scales [15–20]. The range of scales on which perturbation theory works is limited to large scales, which makes it difficult to precisely model the evolved matter density fields [e.g., 21–23]. Recently there have been renewed interest in extending the range of validity of Perturbation Theory

(PT), in the context of Effective field theory of Large Scale Structure [24].

Eisenstein et al. [25] found that the BAO signal was substantially better recovered by displacing galaxies back to nearly initial Lagrangian positions. They measured the displacement field using the inverse Zel'dovich approximation (ZA) applied to the smoothed density fields. Ref. [26] showed that the reconstruction reduced the mode-coupling effect and the BAO signature was much better recovered with a perturbative approach. Ref. [27] used N-body simulations to measure the cross correlation between initial and final density field, known as a propagator, and found that the reconstructed field recovered the initial field at higher k. The BAO reconstruction technique has now been a standard technique of BAO measurements applied to various galaxy surveys [28–34]. There are a number of planned galaxy surveys such as PFS[35], DESI [36], HETDEX[37], Euclid[38], and WFIRST[39] in which the BAO reconstruction technique will be applied.

What about PT after reconstruction? Does the range of scales on which PT works extend to smaller scale than before reconstruction? To answer these issues, we derive the exact perturbative formula of the reconstructed matter power spectrum at one-loop order. Precise theoretical modeling based on PT is useful for cosmological studies using reconstructed density field. We use

* chiaki.hikage@ipmu.jp

the standard perturbation theory (SPT) which is a fundamental approach to understand the nonlinear growth of the density field in weakly nonlinear regime [40–49]. We here see how the one-loop order perturbative terms, which are the leading order of nonlinearity in the matter power spectrum, behave after reconstruction by varying the smoothing scale R_s for the smoothed density fields in reconstruction. We also apply our formula to the formalism of regularized power spectra (RegPT) [23, 50]. Comparing with N-body simulations, we investigate the valid range of scales on which SPT and RegPT work for reconstructed matter density field.

We also study the non-Gaussianity in the reconstructed field using the bispectrum. Since the reconstruction effectively reverses the growth of the large-scale structure, non-Gaussianity due to the nonlinear gravity should decrease by reconstruction. We study this issue by comparing the tree-level PT prediction for the reconstructed bispectrum with numerical simulations.

Our study improves on previous works in several respects compared with Padmanabhan et al. and Noh et al. [26, 51]. We include several perturbative terms which are necessary to describe the nonlinearity in the power spectrum. One is the difference of the shift field between the data and random. In the standard reconstruction method developed by [25], the positions of data (e.g., galaxies) are shifted to cancel the effect of bulk flow and thereby the density field for the data becomes zero at linear order. To recover the linear-order density field, uniformly-distributed particles, a so-called "random" set, are also shifted using the same displacement field as used for the data. Since the data are already displaced from the initial positions, the shift field for the data should be evaluated at Eulerian positions rather than Lagrangian positions. On the other hand, the shifts for the random points should be evaluated at Lagrangian positions. Even though the same shift field is used for the data and randoms, the difference of their positions generates additional nonlinearity at the leading order of PT and changes the bispectrum as well as the power spectrum. Schmittfull et al. [52] properly took into account the effect and derived the second-order Eulerian kernel. Another one is the nonlinearity in the smoothed density field to be used to obtain the shift field for reconstruction. In this paper, we explicitly derive the third-order Eulerian kernel for the reconstructed density field for the first time and investigate the effect of the nonlinearity in smoothed density field on the power spectrum. There has been also no explicit comparison of the perturbative formula of the reconstructed spectrum with numerical simulations. In this paper, we study how the one-loop PT works after reconstruction.

This paper is organized as follows: in Section II, perturbative formulae for the power spectrum and bispectrum after reconstruction are presented. We study how the one-loop terms for the power spectrum are altered by applying the reconstruction technique. In Section III, we compare our perturbative formula with N-body simulations and study the range of scales on which PT works. Section IV is devoted to the summary and conclusions. Throughout the paper, we assume a flat Λ CDM model with the random Gaussian initial condition and use the following cosmological parameters based on WMAP7+BAO+H_0 Mean [53]: $\Omega_b = 0.046$, $\Omega_m = 0.273$, $n_s = 0.963$, $h = 0.704$, $\tau = 0.089$, $\sigma_8 = 0.809$.

II. PERTURBATION THEORY

In this section, we derive the perturbative formula based on the SPT to describe the nonlinearity in the real-space matter power spectrum and bispectrum (see also the details of our derivation in Appendix A). We compare the one-loop order contributions from $\langle \delta^{(1)} \delta^{(3)} \rangle$ and $\langle \delta^{(2)} \delta^{(2)} \rangle$ before and after reconstruction. We also apply the 2nd-order Lagrangian Perturbation Theory (2LPT) instead of Zel'dovich approximation (ZA) in reconstruction to study the effect on the one-loop terms of the power spectrum.

A. Standard Perturbation Theory Before Reconstruction

The Eulerian position of a mass element $\mathbf{x}$ and the Lagrangian position $\mathbf{q}$ are related through a displacement field $\mathbf{\Psi}(\mathbf{q})$ as

$$\mathbf{x} = \mathbf{q} + \mathbf{\Psi}(\mathbf{q}). \tag{1}$$

The mass overdensity and its Fourier transform are then written as

$$\delta(\mathbf{x}) = \int \mathbf{dq}\delta_{\mathrm{D}}(\mathbf{x} - \mathbf{q} - \mathbf{\Psi}(\mathbf{q})) - 1, \tag{2}$$

$$\tilde{\delta}_{\mathbf{k}} = \int \mathbf{dq}e^{-i\mathbf{k}\cdot\mathbf{q}}(e^{-i\mathbf{k}\cdot\mathbf{\Psi}(\mathbf{q})} - 1), \tag{3}$$

where δ_{D} is the 3D Dirac delta function. The displacement field evolves according to the following equation

$$\frac{d^2\mathbf{\Psi}}{dt^2} + 2H\frac{d\mathbf{\Psi}}{dt} = -\nabla_{\mathbf{x}}\phi(\mathbf{q} + \mathbf{\Psi}(\mathbf{q})), \tag{4}$$

where $H = \dot{a}/a$ is the time-dependent Hubble parameter, and $\nabla_{\mathbf{x}}$ is the spatial derivative with respect to the Eulerian coordinate. The gravitational potential ϕ is determined by the Poisson equation

$$\nabla_{\mathbf{x}}{}^2\phi(\mathbf{x}) = 4\pi G\bar{\rho}a^2\delta(\mathbf{x}), \tag{5}$$

where G is the gravitational constant, $\bar{\rho}$ is the mean matter density, and a is the scale factor. The velocity field is assumed to be irrotational throughout this paper.

In LPT, the displacement field is expanded perturbatively as

$$\mathbf{\Psi} = \mathbf{\Psi}^{(1)} + \mathbf{\Psi}^{(2)} + \mathbf{\Psi}^{(3)}\cdots, \tag{6}$$

where $\Psi^{(n)}$ has the order of $(\Psi^{(1)})^n$ and each term in Fourier space is given by

$$\tilde{\Psi}_{\mathbf{k}}^{(n)} = \frac{iD^n(z)}{n!} \int \frac{d\mathbf{k}_1 \cdots d\mathbf{k}_n}{(2\pi)^{3n-3}} \delta_D \left(\sum_{j=1}^{n} \mathbf{k}_j - \mathbf{k} \right)$$
$$\times \mathbf{L}^{(n)}(\mathbf{k}_1, ..., \mathbf{k}_n) \tilde{\delta}_{\mathbf{k}_1}^{L} \cdots \tilde{\delta}_{\mathbf{k}_n}^{L}, \quad (7)$$

where $D(z)$ is the linear growth rate at redshift z normalized by $D(z = 0) = 1$ and δ^{L} is the linear density field at $z = 0$. In the Einstein-de Sitter universe, the Lagrangian perturbative kernels are time-independent and analytically given by [54] as

$$\mathbf{L}^{(1)}(\mathbf{k}) = \frac{\mathbf{k}}{k^2}, \quad (8)$$

$$\mathbf{L}^{(2)}(\mathbf{k}_1, \mathbf{k}_2) = \frac{3}{7} \frac{\mathbf{k}}{k^2} (1 - \mu_{1,2}^2), \quad (9)$$

and

$$\mathbf{L}^{(3)}(\mathbf{k}_1, \mathbf{k}_2, \mathbf{k}_3) = \frac{1}{3} \frac{\mathbf{k}}{k^2} \left[\frac{5}{7} (1 - \mu_{1,2}^2)(1 - \mu_{12,3}^2) \right.$$
$$\left. - \frac{1}{3} (1 - 3\mu_{1,2}^2 + 2\mu_{1,2}\mu_{2,3}\mu_{3,1}) + (2 \text{ perm.}) \right]$$
$$+ \mathbf{k} \times \mathbf{T}(\mathbf{k}_1, \mathbf{k}_2, \mathbf{k}_3), \quad (10)$$

where $\mathbf{k} = \mathbf{k}_1 + \cdots + \mathbf{k}_n$, $\mu_{i,j} = \mathbf{k}_i \cdot \mathbf{k}_j / k_i k_j$, and $\mu_{ij,k} = (\mathbf{k}_i + \mathbf{k}_j) \cdot \mathbf{k}_k / |\mathbf{k}_i + \mathbf{k}_j| k_k$. The transverse part $\mathbf{k} \times \mathbf{T}$ is unnecessary in the following application [54]. In more general cosmologies, the above expression is still a good approximation [48], while the exact formula is given by [41, 42, 45].

The perturbation series of the matter overdensity δ is given as

$$\tilde{\delta}_{\mathbf{k}}^{(1)} = -i\mathbf{k} \cdot \tilde{\mathbf{\Psi}}_{\mathbf{k}}^{(1)} = D(z)\tilde{\delta}_{\mathbf{k}}^{L}, \quad (11)$$

$$\tilde{\delta}_{\mathbf{k}}^{(n)} = D^n(z) \int \frac{d\mathbf{k}_1 \cdots d\mathbf{k}_n}{(2\pi)^{3n-3}} \delta_D \left(\sum_{j=1}^{n} \mathbf{k}_j - \mathbf{k} \right)$$
$$\times F_n(\mathbf{k}_1, \cdots, \mathbf{k}_n) \tilde{\delta}_{\mathbf{k}_1}^{L} \cdots \tilde{\delta}_{\mathbf{k}_n}^{L}, \quad (12)$$

where F_n is the n-th order Eulerian perturbative kernel. Following the previous literature [e.g., 42, 45], the symmetrization factor $1/n!$ is not included in the definition of the Eulerian kernel, while it is included in that of the Lagrangian kernel (eq.[7]). The second- and third-order Eulerian kernels are given by [41, 42, 45]

$$F_2(\mathbf{k}_1, \mathbf{k}_2) = \frac{1}{2} [\mathbf{k} \cdot \mathbf{L}^{(2)}(\mathbf{k}_1, \mathbf{k}_2) + (\mathbf{k} \cdot \mathbf{L}^{(1)}(\mathbf{k}_1))(\mathbf{k} \cdot \mathbf{L}^{(1)}(\mathbf{k}_2))]$$
$$= \frac{5}{7} + \frac{2}{7} \left(\frac{\mathbf{k}_1 \cdot \mathbf{k}_2}{k_1 k_2} \right)^2 + \frac{\mathbf{k}_1 \cdot \mathbf{k}_2}{2k_1 k_2} \left(\frac{k_2}{k_1} + \frac{k_1}{k_2} \right), \quad (13)$$

and

$$F_3(\mathbf{k}_1, \mathbf{k}_2, \mathbf{k}_3) = \frac{1}{6} \left[\mathbf{k} \cdot \mathbf{L}^{(3)}(\mathbf{k}_1, \mathbf{k}_2, \mathbf{k}_3) \right.$$
$$+ (\mathbf{k} \cdot \mathbf{L}^{(1)}(\mathbf{k}_1))(\mathbf{k} \cdot \mathbf{L}^{(1)}(\mathbf{k}_2))(\mathbf{k} \cdot \mathbf{L}^{(1)}(\mathbf{k}_3))$$
$$\left. + \left\{ (\mathbf{k} \cdot \mathbf{L}^{(1)}(\mathbf{k}_1))(\mathbf{k} \cdot \mathbf{L}^{(2)}(\mathbf{k}_2, \mathbf{k}_3)) + (2 \text{ perms.}) \right\} \right]. \quad (14)$$

The matter power spectrum $P(k)$ is defined as

$$\langle \tilde{\delta}_{\mathbf{k}} \tilde{\delta}_{\mathbf{k}'} \rangle \equiv (2\pi)^3 \delta_D(\mathbf{k} + \mathbf{k}') P(k). \quad (15)$$

The power spectrum up to one-loop order is given by

$$P(k, z) = D^2(z) P_{11}(k) + D^4(z)[P_{22}(k) + P_{13}(k)], \quad (16)$$

where P_{nm} is the contribution from $\langle \tilde{\delta}_{\mathbf{k}}^{(n)} \tilde{\delta}_{\mathbf{k}}^{(m)} \rangle$. The leading order term is the linear power spectrum

$$P_{11}(k) = P_L(k), \quad (17)$$

and the next-leading order terms are the following two one-loop terms:

$$P_{22}(k) = 2 \int \frac{d\mathbf{p}}{(2\pi)^3} P_L(|\mathbf{k} - \mathbf{p}|) P_L(p) [F_2(\mathbf{k} - \mathbf{p}, \mathbf{p})]^2,$$
$$= \frac{1}{98} \frac{k^3}{4\pi^2} \int_0^{\infty} dr P_L(kr) \int_{-1}^{1} dx P_L(k_*)$$
$$\times \frac{(3r + 7x - 10rx^2)^2}{(1 + r^2 - 2rx)^2}, \quad (18)$$

where $k_* \equiv k(1 + r^2 - 2rx)^{1/2}$ and

$$P_{13}(k) = 6P_L(k) \int \frac{d\mathbf{p}}{(2\pi)^3} P_L(p) F_3(\mathbf{k}, \mathbf{p}, -\mathbf{p}),$$
$$= \frac{1}{252} \frac{k^3}{4\pi^2} P_L(k) \int_0^{\infty} dr P_L(kr) \left[\frac{12}{r^2} - 158 + 100r^2 \right.$$
$$\left. - 42r^4 + \frac{3}{r^3} (r^2 - 1)^3 (7r^2 + 2) \ln \left| \frac{1+r}{1-r} \right| \right]. \quad (19)$$

The bispectrum at the tree-level order is given by

$$B(k_1, k_2, k_3) = 2F_2(\mathbf{k}_1, \mathbf{k}_2) D^4(z) P_L(k_1) P_L(k_2) + (2 \text{ perms.}). \quad (20)$$

B. Standard Perturbation Theory After Reconstruction

Next we move to the reconstructed field. To reconstruct the density field, we shift the observed particle positions to correct the bulk flow motion following the procedure of [25]. When the shift field $\mathbf{s}$ is computed from the negative ZA [55] of the smoothed density field, it is obtained by

$$\tilde{\mathbf{s}}_{\mathbf{k}} = -iW(k)\mathbf{L}^{(1)}(\mathbf{k})\tilde{\delta}_{\mathbf{k}}, \quad (21)$$

where $W(k)$ is the smoothing kernel. We adopt a Gaussian kernel $W(k) = \exp(-k^2 R_s^2 / 2)$, varying the smoothing scale of R_s throughout the paper. Since the shift field is computed from the negative ZA of the smoothed density field (eq.21), the perturbative series of the shift field is given by that of the smoothed density field as

$$\tilde{\mathbf{s}}_{\mathbf{k}}^{(n)} = -iW(k)\mathbf{L}^{(1)}(\mathbf{k})\tilde{\delta}_{\mathbf{k}}^{(n)}. \quad (22)$$

This can be rewritten in a similar form to the Lagrangian kernel (eq. 7) as

$$\tilde{\mathbf{s}}_{\mathbf{k}}^{(n)} = \frac{iD^n(z)}{n!} \int \frac{d\mathbf{k}_1 \cdots d\mathbf{k}_n}{(2\pi)^{3n-3}} \delta_{\mathrm{D}} \left(\sum_{j=1}^{n} \mathbf{k}_j - \mathbf{k} \right)$$
$$\times \mathbf{S}^{(n)}(\mathbf{k}_1, ..., \mathbf{k}_n) \tilde{\delta}_{\mathbf{k}_1}^{\mathrm{L}} \cdots \tilde{\delta}_{\mathbf{k}_n}^{\mathrm{L}}, \qquad (23)$$

where the kernel of the shift field $\mathbf{S}^{(n)}$ is given by

$$\mathbf{S}^{(n)}(\mathbf{k}_1, ..., \mathbf{k}_n) = -n! W(k) \mathbf{L}^{(1)}(\mathbf{k}) F_n(\mathbf{k}_1, ..., \mathbf{k}_n). \quad (24)$$

At linear order, $\mathbf{S}^{(1)}$ becomes $-W(k)\mathbf{L}^{(1)}$ and thereby the displacement due to gravitational evolution is canceled out by reconstruction on large scales ($W(k) \simeq 1$), i.e., $\tilde{\mathbf{\Psi}}_{\mathbf{k}}^{(1)} + \tilde{\mathbf{s}}_{\mathbf{k}}^{(1)} \simeq 0$. At higher order, however, they are not completely canceled out with each other even on large scales.

The displaced density field is written as

$$\tilde{\delta}_{\mathbf{k}}^{(\mathrm{d})} = \int d\mathbf{q} e^{-i\mathbf{k}\cdot\mathbf{q}} (e^{-i\mathbf{k}\cdot[\mathbf{\Psi}(\mathbf{q})+\mathbf{s}(\mathbf{x})]} - 1), \qquad (25)$$

where the shift field of the evolved mass particles is evaluated at the Eulerian positions $\mathbf{s}(\mathbf{x})$ rather than at the Lagrangian position $\mathbf{s}(\mathbf{q})$, as discussed in [52]. The difference of the shift field between the Eulerian positions $\mathbf{x}$ and Lagrangian positions $\mathbf{q}$ is perturbatively expanded in terms of $\mathbf{\Psi}$ as

$$\mathbf{s}(\mathbf{x}) = \int \frac{d\mathbf{k}}{(2\pi)^3} \tilde{\mathbf{s}}_{\mathbf{k}} \, e^{i\mathbf{k}\cdot(\mathbf{q}+\mathbf{\Psi}(\mathbf{q}))}, \qquad (26)$$

$$= \sum_{n=0}^{\infty} \int \frac{d\mathbf{k}}{(2\pi)^3} \tilde{\mathbf{s}}_{\mathbf{k}} \, e^{i\mathbf{k}\cdot\mathbf{q}} \left[\frac{1}{n!}(i\mathbf{k}\cdot\mathbf{\Psi}(\mathbf{q}))^n \right],$$

$$= \mathbf{s}(\mathbf{q}) + (\mathbf{\Psi}(\mathbf{q})\cdot\nabla)\mathbf{s}(\mathbf{q}) + \frac{1}{2}(\mathbf{\Psi}(\mathbf{q})\cdot\nabla)^2 \mathbf{s}(\mathbf{q}) \cdots. \qquad (27)$$

The shifted density field of a spatially uniform grid or random is given by

$$\tilde{\delta}_{\mathbf{k}}^{(\mathrm{s})} = \int d\mathbf{q} e^{-i\mathbf{k}\cdot\mathbf{q}} (e^{-i\mathbf{k}\cdot\mathbf{s}(\mathbf{q})} - 1), \qquad (28)$$

where the shift field of the (unevolved) uniform grid is evaluated at the Lagrangian position. The reconstructed density field is given as

$$\tilde{\delta}_{\mathbf{k}}^{(\mathrm{rec})} \equiv \tilde{\delta}_{\mathbf{k}}^{(\mathrm{d})} - \tilde{\delta}_{\mathbf{k}}^{(\mathrm{s})}$$
$$= \int d\mathbf{q} e^{-i\mathbf{k}\cdot\mathbf{q}} e^{-i\mathbf{k}\cdot\mathbf{s}(\mathbf{q})} (e^{-i\mathbf{k}\cdot[\mathbf{\Psi}(\mathbf{q})+\mathbf{s}(\mathbf{x})-\mathbf{s}(\mathbf{q})]} - 1). \qquad (29)$$

At linear order, the reconstructed density field is unaltered as

$$\delta_{\mathbf{k}}^{(\mathrm{rec})(1)} = \delta_{\mathbf{k}}^{(1)}. \qquad (30)$$

There is a difference in higher-order terms of $\delta^{(\mathrm{rec})}$

$$\tilde{\delta}_{\mathbf{k}}^{(\mathrm{rec})(n)} = D^n(z) \int \frac{d\mathbf{k}_1 \cdots d\mathbf{k}_n}{(2\pi)^{3n-3}} \delta_{\mathrm{D}} \left(\sum_{j=1}^{n} \mathbf{k}_j - \mathbf{k} \right)$$
$$\times F_n^{(\mathrm{rec})}(\mathbf{k}_1, ..., \mathbf{k}_n) \tilde{\delta}_{\mathbf{k}_1}^{\mathrm{L}} \cdots \tilde{\delta}_{\mathbf{k}_n}^{\mathrm{L}}, \qquad (31)$$

where $F_n^{(\mathrm{rec})}$ is the Eulerian kernel for the reconstructed matter density field. In this paper, we derive $F_n^{(\mathrm{rec})}$ up to third order by expanding the reconstructed density fields (eq. 29) perturbatively. The detail of derivations is summarized in Appendix A. The second-order Eulerian kernel for the reconstructed field $F_2^{(\mathrm{rec})}$ becomes

$$F_2^{(\mathrm{rec})}(\mathbf{k}_1, \mathbf{k}_2) = F_2(\mathbf{k}_1, \mathbf{k}_2)$$
$$+ \frac{1}{2} \left[(\mathbf{k}\cdot\mathbf{S}^{(1)}(\mathbf{k}_1)) + (\mathbf{k}\cdot\mathbf{S}^{(1)}(\mathbf{k}_2)) \right],$$
$$= \frac{5}{7} - \frac{W_1 + W_2}{2} + \frac{2}{7}\left(\frac{\mathbf{k}_1\cdot\mathbf{k}_2}{k_1 k_2} \right)^2$$
$$+ \left(\frac{\mathbf{k}_1\cdot\mathbf{k}_2}{2k_1 k_2} \right) \left[\frac{k_2}{k_1}(1 - W_1) + \frac{k_1}{k_2}(1 - W_2) \right], \qquad (32)$$

where F_n without upperscript of (rec) denotes the n-th order Eulerian kernel without reconstruction (eq. 13) and $W_i \equiv W(k_i)$. The third-order kernel becomes

$$F_3^{(\mathrm{rec})}(\mathbf{k}_1, \mathbf{k}_2, \mathbf{k}_3) = F_3(\mathbf{k}_1, \mathbf{k}_2, \mathbf{k}_3)$$
$$+ \frac{1}{6}\left[2(\mathbf{k}\cdot\mathbf{S}^{(1)}(\mathbf{k}_1))F_2(\mathbf{k}_2, \mathbf{k}_3) \right.$$
$$+ (\mathbf{k}\cdot\mathbf{S}^{(1)}(\mathbf{k}_1))(\mathbf{k}\cdot\mathbf{S}^{(1)}(\mathbf{k}_2))$$
$$\left. + (\mathbf{k}\cdot\mathbf{S}^{(2)}(\mathbf{k}_1, \mathbf{k}_2)) + (2 \text{ perms.}) \right], \qquad (33)$$

where $\mathbf{k}_{ij} \equiv \mathbf{k}_i + \mathbf{k}_j$ and $W_{ij} \equiv W(|\mathbf{k}_{ij}|)$. The last term including the $\mathbf{S}^{(2)}$ kernel comes from the second-order nonlinearity of the shift field $\mathbf{s}(\mathbf{x})$.

At linear order, the power spectrum is unchanged by reconstruction as shown in the equation (30). The one-loop terms for the matter power spectrum are altered as

$$P_{22}^{(\mathrm{rec})}(k) = 2 \int \frac{d\mathbf{p}}{(2\pi)^3} P_{\mathrm{L}}(|\mathbf{k}-\mathbf{p}|) P_{\mathrm{L}}(p) [F_2^{(\mathrm{rec})}(\mathbf{k}-\mathbf{p}, \mathbf{p})]^2,$$
$$= \frac{1}{98} \frac{k^3}{4\pi^2} \int_0^{\infty} dr P_L(kr) \int_{-1}^{1} dx P_L(k_*)$$
$$\times \left[\frac{3r + 7x - 10rx^2 - 7W_{k_*}r(1-rx)}{1 + r^2 - 2rx} - 7W_{kr}x \right]^2, \qquad (34)$$

where $k_* = k(1 + r^2 - 2rx)^{1/2}$ and

$$
\begin{aligned}
P_{13}^{(\mathrm{rec})}(k) &= 6P_{\mathrm{L}}(k) \int \frac{d\mathbf{p}}{(2\pi)^3} P_{\mathrm{L}}(p) F_3^{(\mathrm{rec})}(\mathbf{k}, \mathbf{p}, -\mathbf{p}), \\
&= P_{13}(k) + \frac{k^3}{4\pi^2} P_L(k) \int_0^\infty dr P_L(kr) \\
&\quad \times \left[\frac{2}{3}(2W_{kr} - W_{kr}^2 + 2r^2 W_{kr}) \right. \\
&\quad \left. - \int_{-1}^1 dx\, \frac{2r(1-rx)(10r + 4rx^2 - 7r^2x - 7x)}{7(1 + r^2 - 2rx)} W_{k_*} \right].
\end{aligned}
$$
(35)

The tree-level bispectrum for the reconstructed matter density field is also obtained by replacing F_2 with $F_2^{(\mathrm{rec})}$ as

$$
\begin{aligned}
B(k_1, k_2, k_3) &= 2F_2^{(\mathrm{rec})}(\mathbf{k}_1, \mathbf{k}_2) D^4(z) P_{\mathrm{L}}(k_1) P_{\mathrm{L}}(k_2) \\
&\quad + (2\ \mathrm{perms.}).
\end{aligned}
$$
(36)

C. Power Spectrum Before and After reconstruction

Let's see how the one-loop contributions of the power spectrum change after reconstruction. Figure 1 shows the comparison of the one-loop components $P_{22}(k)$ and $P_{13}(k)$ before and after reconstruction with different R_s. After reconstruction, the amplitude of the P_{22} term substantially decreases even at high k and the decrement is more significant at smaller R_s. This indicates that the reconstruction significantly reduces the mode-coupling effect due to nonlinear gravity. One can understand how P_{22} decreases from the equation for the F_2 kernel (eq. 32). On very large scales ($W(k) \to 1$), the final term in the right-hand side cancels out by reconstruction. This term corresponds to the nonlinearity due to the shift term $\Psi^{(1)} \cdot \Delta \delta^{(1)}$, which encodes the motion of the density perturbations due to the gravitational potential [52, 56].

The other one-loop term $P_{13}(k)$, which has in-phase BAO oscillations but with negative amplitude, contributes to suppress the intrinsic BAO signature. The magnitude of the reconstructed $P_{13}(k)$ also decreases when the smoothed density field is close to linear, which corresponds to $R_s \gtrsim 10h^{-1}\mathrm{Mpc}$. Since the amplitude of P_{13} decreases, the BAO signature is substantially recovered. When the value of R_s is smaller than $10h^{-1}\mathrm{Mpc}$, however, the negative amplitude of $P_{13}(k)$ increases on scales $k < R_s^{-1}$, which again causes degradation of the BAO signal. The effect increases as R_s reduces. This indicates that the behaviour comes from the nonlinearity in the smoothed density field $\mathbf{s}$ given by the $\mathbf{S}^{(2)}$ term in equation (33). In the next subsection, we work on this issue by applying the 2nd-order Lagrangian Perturbation Theory (2LPT) reconstruction instead of ZA.

The upper-right panel in Figure 1 shows the net contributions of one-loop terms. Since the one-loop components are largely canceled out by each other, the net contribution is much smaller than the amplitude of the individual one-loop terms. When reconstructing with $R_s \sim 10h^{-1}\mathrm{Mpc}$, the net contribution is also smaller than the unreconstructed case. For $R_s \lesssim 10h^{-1}\mathrm{Mpc}$, however, the net contribution becomes negative on $k < R_s^{-1}$ because the negative amplitude of P_{13} increases. The lower-right panel in Figure 1 shows the power spectrum including the one-loop components normalized by a no-wiggle spectrum $P_{\mathrm{nw}}(k)$, calculated from the no-wiggle formula of the linear spectrum in [57]. Since the one-loop components become smaller after reconstruction, one can see that the reconstructed spectrum approaches the linear one compared with the unreconstructed spectrum. When R_s is less than $10h^{-1}\mathrm{Mpc}$, the reconstructed power spectrum is below the linear power spectrum on large scale ($k < R_s^{-1}$) but again surpasses the linear one as k increases.

D. Reconstruction using 2LPT

In the previous subsection, we find that the negative amplitude of P_{13} increases and the deviation from the linear spectrum increases when the scale R_s of the smoothed density field to be used for reconstruction is smaller. We confirm that this behaviour comes from the nonlinearity in the smoothing density field by comparing the 2LPT reconstruction with the ZA reconstruction.

When the shift field is computed based on 2LPT [27, 58], it is given in terms of the gravitational potential ϕ as

$$
\mathbf{s} = -\nabla \phi^{(1)} + \frac{3}{7} \nabla \phi^{(2)}.
$$
(37)

The first term in the right-hand side represents the ZA approximation and then the potential $\phi^{(1)}$ is computed from the smoothed density field $\delta^{(\mathrm{smoothed})}$ using the following relation:

$$
\nabla^2 \phi^{(1)} = \delta^{(\mathrm{smoothed})}.
$$
(38)

The second term in the equation (37) corresponds to the 2LPT correction term and then the potential $\phi^{(2)}$ is computed from $\phi^{(1)}$ as

$$
\nabla^2 \phi^{(2)} = \frac{1}{2} \sum_{i \neq j} \left\{ \phi_{,ii}^{(1)} \phi_{,jj}^{(1)} - [\phi_{,ij}^{(1)}]^2 \right\},
$$
(39)

where i, j denote x, y and z. Note that the smoothed density field $\delta^{(\mathrm{smoothed})}$ is not completely linear and thereby the ZA potential $\phi^{(1)}$ includes the nonlinearity. In order to remove the 2nd-order nonlinearity, we use a positive sign of the 2nd-order correction.

In Fourier space, the shift field (eq. 21) is then modified to be

$$
\begin{aligned}
\tilde{\mathbf{s}}_{\mathbf{k}} &= -iW(k)\mathbf{L}^{(1)}(\mathbf{k})\tilde{\delta}_{\mathbf{k}} + \frac{i}{2} \int \frac{d\mathbf{k}_1 d\mathbf{k}_2}{(2\pi)^3} \delta_{\mathrm{D}}(\mathbf{k}_1 + \mathbf{k}_2 - \mathbf{k}) \\
&\quad \times W_1 W_2 \mathbf{L}^{(2)}(\mathbf{k}_1, \mathbf{k}_2) \tilde{\delta}_{\mathbf{k}_1} \tilde{\delta}_{\mathbf{k}_2},
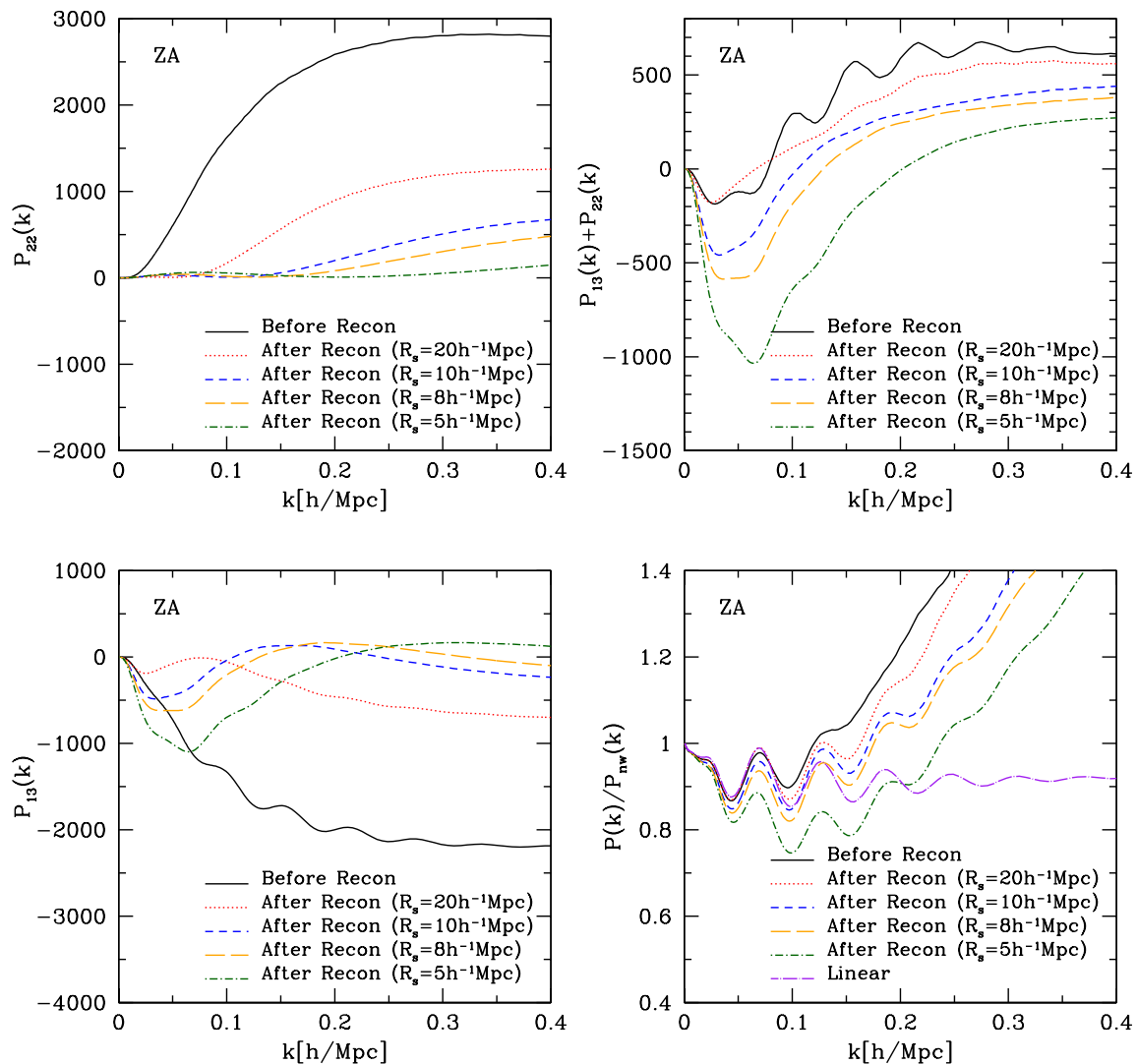\end{aligned}
$$
(40)

FIG. 1. Comparison of the one-loop components $P_{22}(k)$ (upper left), $P_{13}(k)$ (lower left), their sum (upper right), and the matter power spectrum including the one-loop components normalized with the no-wiggle components $P_{\rm nw}$ (lower right). The solid line denotes the result before reconstruction while other lines show the results after reconstruction with different $R_s = 20h^{-1}{\rm Mpc}$ (dotted lines), $10h^{-1}{\rm Mpc}$ (short-dashed lines), $8h^{-1}{\rm Mpc}$ (long-dashed lines) and $5h^{-1}{\rm Mpc}$ (dot-dashed lines). The displacement field in reconstruction is computed with the inverse ZA of the smoothed density field with a Gaussian filter at different smoothing scales R_s (eq. 21).

The second-order kernel for the shift field in the 2LPT reconstruction is altered to

$$\mathbf{S}^{(2)}(\mathbf{k}_1, \mathbf{k}_2) \to \mathbf{S}^{(2)}(\mathbf{k}_1, \mathbf{k}_2) + W_1 W_2 \mathbf{L}^{(2)}(\mathbf{k}_1, \mathbf{k}_2). \quad (41)$$

On large scales where W_1 and W_2 are close to unity, the $\mathbf{L}^{(2)}$ term included in $\mathbf{S}^{(2)}$ is completely canceled out and thereby the nonlinearity decreases. One of the one-loop terms, P_{22}, remains the same; however, the other term

P_{13} changes to

$$P_{13}^{(\rm rec,2LPT)}(k) = P_{13}^{(\rm rec)}(k) + \frac{k^3}{4\pi^2} P_L(k) \int_0^\infty dr P_L(kr)$$

$$\times \int_{-1}^1 dx \frac{6r^2(1-rx)(1-x^2)}{7(1+r^2-2rx)} W_k W_{kr}. \quad (42)$$

Figure 2 shows the results of $P_{13}(k)$ and the 1-loop SPT power spectrum by reconstruction with 2LPT. When reconstructing with 2LPT, the negative amplitude that appeared at small k becomes smaller in magnitude and as a result the power spectrum is closer to the linear spectrum than when reconstructing using ZA. The difference from
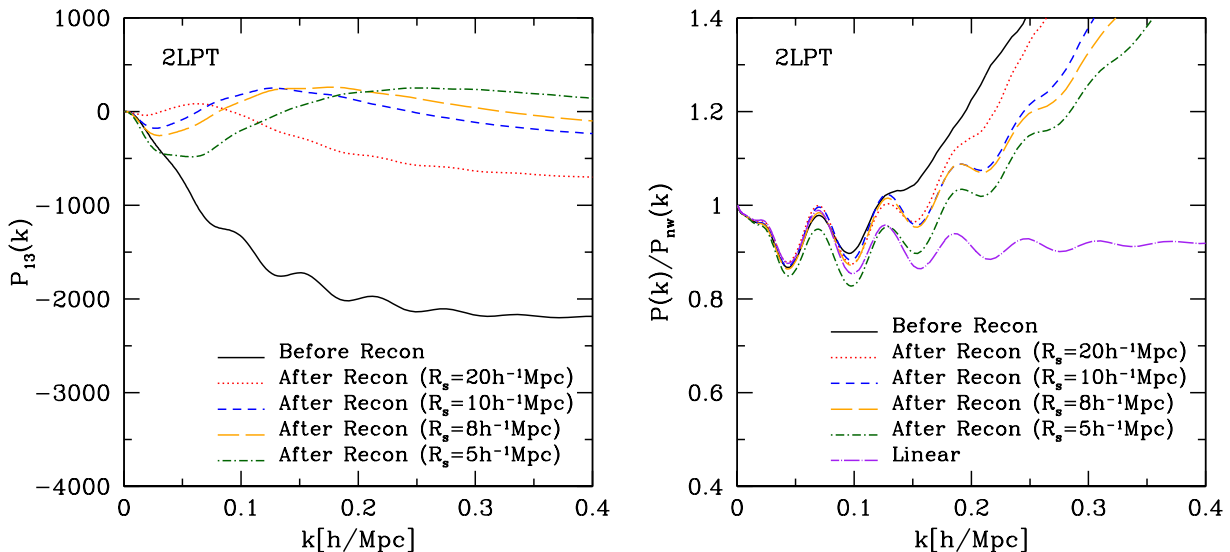
FIG. 2. Same as the lower two panels in Fig. 1 but for the 2LPT reconstruction.

the reconstruction in ZA comes from the second-order kernel for the shift field $\mathbf{S}^{(2)}$ in the equation (41). Our result indicates that the nonlinearity in the smoothed density field $\mathbf{S}^{(2)}$ causes the negative amplitude of $P_{13}(k)$ on small k.

III.   COMPARISON OF PERTURBATION THEORY WITH N-BODY SIMULATIONS

We run N-body simulations to generate the reconstructed matter density field. We compare the perturbative formula of matter power spectrum and bispectrum derived in the previous section with the numerical results to study the range of scales in which PT works.

A.   N-body simulations

We use the publicly available cosmological N-body simulation code Gadget-2 [16]. The mass particles are initially distributed using the 2LPT code [59] with Gaussian initial conditions at the initial redshift of 49. The simulation is performed in a periodic cubic box with side length $1h^{-1}$Gpc, with 800^3 particles each of mass $1.3 \times 10^{11} h^{-1} M_\odot$.

The simulated mass density field δ is evaluated on an 800^3 cubic lattice, using Clouds-in-Cell (CIC) assignment. We compute the shift field $\mathbf{s}(\mathbf{x}_i)$ at each grid point $\mathbf{x}_i$ as follows: Fourier transforming $\delta(\mathbf{x}_i)$ using the Fast Fourier transform (FFT) method, multiplying $\delta(\mathbf{k})$ by $-i\mathbf{k}/k^2 W(kR_s)$, and transforming back to real space. Each mass particle position $\mathbf{x}$ is shifted to $\mathbf{x} + \mathbf{s}(\mathbf{x})$

where $\mathbf{s}(\mathbf{x})$ is linearly interpolated from the shift vectors at the neighboring pixels, and we recompute the shifted density field $\delta^{(\mathrm{d})}$. The shifted random (uniform grid) field $\delta^{(\mathrm{s})}$ is obtained by shifting each grid position by $\mathbf{s}(\mathbf{x}_i)$. Matter power spectra are computed in Fourier space by linearly binning with $\Delta k = 0.01h/$Mpc. The calculation of bispectra is also performed in Fourier space focused on some specific triangle configurations: $(k_1, k_2) = (0.05, 0.1), (0.1, 0.2), (0.15, 0.3)$ and $(0.2, 0.4)$ in unit of h^{-1}Mpc where the binning width of k_1 and k_2 $0.01h^{-1}$Mpc and their opening angle θ varies from 0 to π with a binning width of $\pi/15$. We run 10 realizations to evaluate the errors of the power spectrum and bispectrum. When comparing PT with the numerical results, the CIC pixel window function is added to the Gaussian smoothing $W(k)$ in the calculation of PT.

B.   Power Spectrum

Figure 3 shows the comparison of the one-loop SPT with the N-body results averaged over 10 realizations at $z = 0.3$ (left) and $z = 1$ (right). The top panels are the results before reconstruction and the other panels show the results after reconstruction with different R_s. Before reconstruction, the one-loop SPT is in good agreement with the N-body results in the weakly nonlinear regime ($k \lesssim 0.1h^{-1}$Mpc) with errors around one percent, while the SPT overestimates the matter power at higher k. This behaviour is consistent with the previous works [e.g., 22, 49]. After reconstruction, the simulated matter power spectrum approaches the linear spectrum for $R_s \gtrsim 10h^{-1}$Mpc. We find that one-loop SPT agrees with the N-body results after reconstruction in the weakly
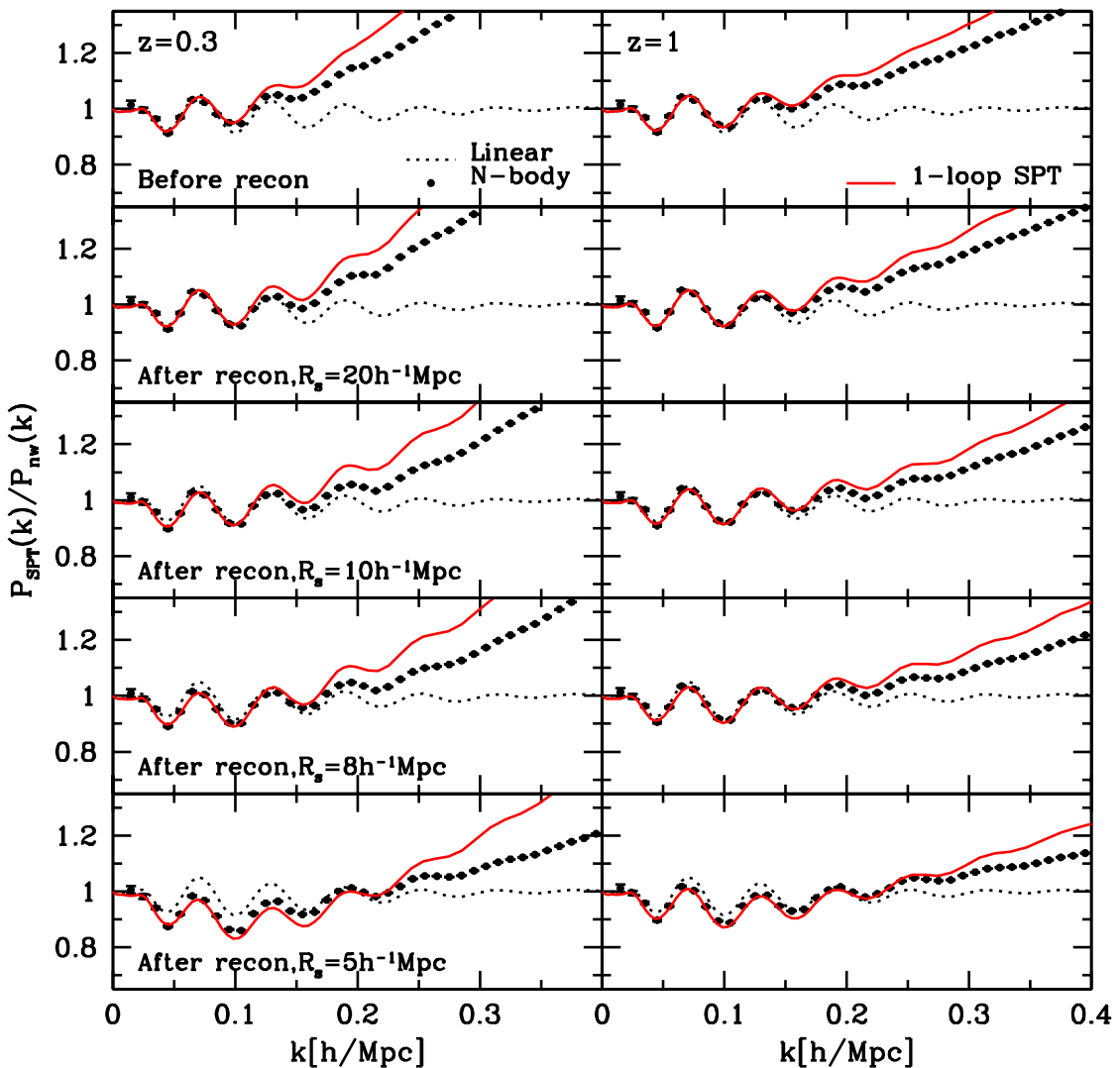
FIG. 3. Matter power spectrum computed from N-body simulations (filled circles) before reconstruction (top) and after reconstruction with different $R_s = 20, 10, 8$ and $5h^{-1}$Mpc (from second-top to bottom). The output redshift is $z = 0.3$ (left) and $z = 1$ (right). The matter power spectra are normalized with the no-wiggle spectra at the corresponding redshift. The error-bars represent the 1σ dispersion of our simulation results. Lines represent the linear power spectrum (dotted lines) and 1-loop SPT (solid lines).

nonlinear regime, while PT still overestimates in nonlinear regime. The agreement of the one-loop PT with the N-body results is better up to larger k than the prereconstruction case when R_s is chosen to be $8-10h^{-1}$Mpc. This indicates that the nonlinear gravity effect becomes smaller by reconstruction and thereby the range of scales on which PT holds extends to larger k. As R_s is larger, the reconstruction becomes ineffective because the reconstuction only corrects the bulk motion at scales larger than around R_s. The limit that R_s goes infinity corresponds to no reconstruction.

When R_s is smaller than $10h^{-1}$Mpc, the deviation from the linear spectrum increases at small k. This behaviour is consistent with the predictions from PT that the net ampltitude of the one-loop terms increase on large scale. When $R_s = 5h^{-1}$Mpc, there is a deviation between PT and the numerical results on relatively large scale ($k \sim 0.1h^{-1}$Mpc). This comes from that the nonlinearity in the smoothed density field becomes significant for small R_s and thereby PT breaks down even for large scale modes, as discussed in the previous section. Nevertheless, the deviation becomes smaller at higher redshift
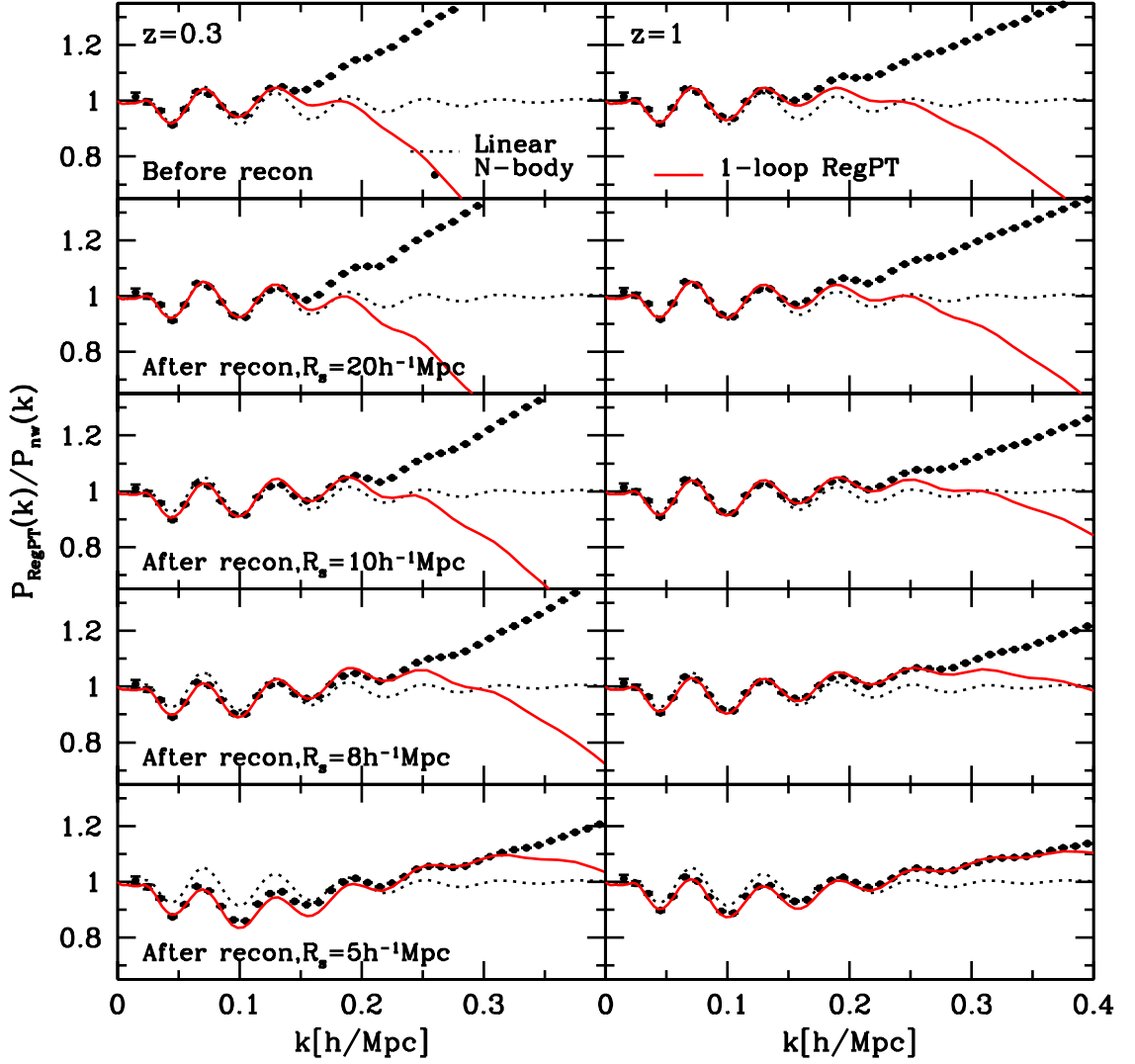
FIG. 4. Same as Fig. 3 but for the comparison of the one-loop RegPT predictions.

and then the agreement between PT and the numerical results holds up to much larger k than before reconstruction.

We also apply the regularized power spectrum (RegPT) to describe the power spectrum for the reconstructed field. RegPT is an improved PT in which the SPT is reorganized with the multi-point propagators [21, 23, 60]. Analytical expression up to one-loop order is given by [23] as

$$
P(k; \eta) = [\Gamma_{\rm reg}^{(1)}(k; \eta)]^2 P_0(k)
$$
$$
+ 2 \int \frac{d\mathbf{q}}{(2\pi)^3} [\Gamma_{\rm reg}^{(2)}(\mathbf{q}, \mathbf{k} - \mathbf{q}; \eta)]^2 P_0(q) P_0(|\mathbf{k} - \mathbf{q}|),
$$
$$(43)$$

where $\eta \equiv \ln D(t)$ and the multi-point propagators $\Gamma_{\rm reg}^{(n)}$ are

$$
\Gamma_{\rm reg}^{(1)}(k; \eta) = e^\eta \left[1 + \frac{k^2 \sigma_d^2 e^{2\eta}}{2} + e^{2\eta} \bar\Gamma_{1-\rm loop}^{(1)}(k) \right]
$$
$$
\times \exp \left\{ -\frac{k^2 \sigma_d^2 e^{2\eta}}{2} \right\},
$$
$$(44)$$

$$
\Gamma_{\rm reg}^{(2)}(\mathbf{q}, \mathbf{k} - \mathbf{q}; \eta) = e^{2\eta} F_2(\mathbf{q}, \mathbf{k} - \mathbf{q}) \exp \left\{ -\frac{k^2 \sigma_d^2 e^{2\eta}}{2} \right\},
$$
$$(45)$$

and

$$
\bar\Gamma_{1-\rm loop}^{(1)}(k) = 3 \int \frac{d\mathbf{q}}{(2\pi)^3} F_3(\mathbf{q}, -\mathbf{q}, \mathbf{k}) P_0(q).
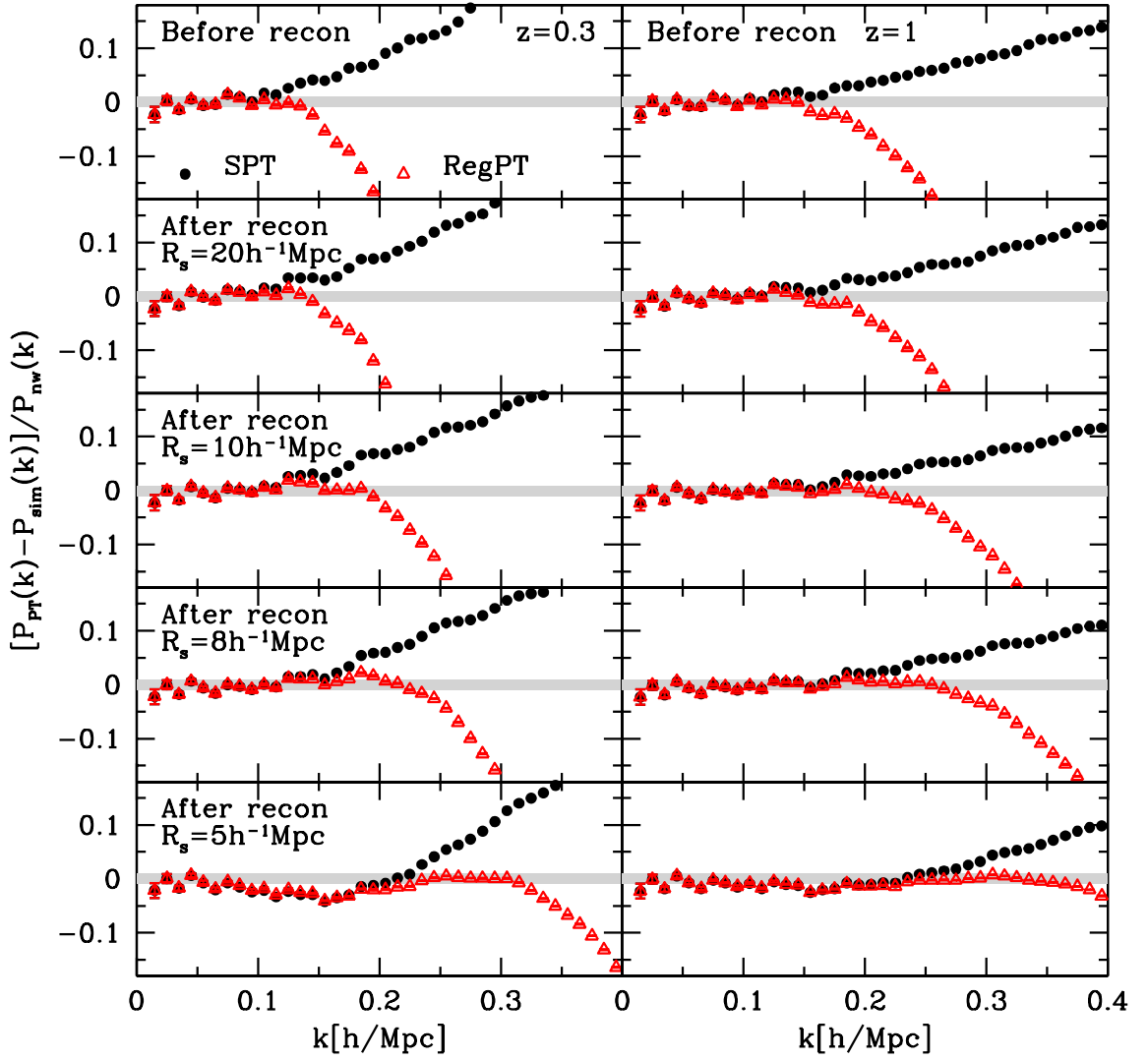$$
$$(46)$$

FIG. 5. Deviation of the one-loop PT of matter power spectrum (SPT with filled circles and RegPT with open triangles) from N-body results before reconstruction (top) and after reconstruction with different R_s from $20, 10, 8$ and $5h^{-1}$Mpc (second top to bottom). The redshift is $z = 0.3$ (left) and $z = 1$ (right). The shaded area indicates $\pm 1\%$ range of the deviation.

We obtain the RegPT formula for the reconstructed spectrum by replacing the Eulerian kernels F_n with $F_n^{(\text{rec})}$ (eq. 32 for $n = 2$ and eq. 33 for $n = 3$). The σ_d represents the dispersion of the displacement field

$$\sigma_d^2(k) = \int_0^{k_\Lambda(k)} \frac{d\mathbf{q}}{6\pi^2} P_L(\mathbf{q}), \qquad (47)$$

where the running UV cutoff $k_\Lambda(k)$ is set to be $k/2$ by [23]. Since the Lagrangian displacement becomes effectively smaller by reconstruction [26], the value of $\sigma_d^2(k)$ should be smaller after reconstruction. We then set $(\sigma_d^2(k))^{\text{recon}} = b\sigma_d^2(k)$ with b treated as a free parameter to fit the simulated spectrum.

Figure 4 shows the comparison of the one-loop RegPT power spectrum with the simulated results at $z = 0.3$ (left) and $z = 1$ (right). Similar to Figure 3, the top panels show the results before reconstruction and the other panels are the results after reconstruction with different R_s. RegPT describes the matter power spectrum better than the SPT at one-loop level. On nonlinear scales, RegPT underestimates the matter power spectrum due to the exponential damping for the dispersion of the displacement (eq. 47). After reconstruction, we find that the smaller value of b is better fitted to the N-body re-

sults at smaller R_s: $b = 1$ for $R_s = 20h^{-1}$Mpc, $b = 0.7$ for $R_s = 10h^{-1}$Mpc, $b = 0.5$ for $R_s = 8h^{-1}$Mpc, and $b = 0.3$ for $R_s = 5h^{-1}$Mpc. When R_s is around $8h^{-1}$Mpc, the agreement between one-loop RegPT and the N-body results reaches up to the third BAO peak ($k \sim 0.18h$/Mpc) at $z = 0.3$ and the fourth BAO peak ($k \sim 0.24h$/Mpc) at $z = 1$.

Figure 5 shows the deviation of the power spectrum between PT and N-body simulations normalized with the no-wiggle components $[(P_{\rm PT}(k) - P_{\rm sim}(k))/P_{\rm nw}(k)]$. The gray shaded area represents the 1 percent range of the deviation. Before reconstruction, the agreement of the one-loop RegPT with the simulations is good up to around $0.1h^{-1}$Mpc within 1% error. After reconstruction, their agreement extends up to $0.2 - 0.25\,h$Mpc^{-1} when R_s chosen to be $8 - 10h^{-1}$Mpc. Our results indicate that the higher-order mode-coupling beyond the one-loop order becomes smaller by reconstruction and then the agreement of PT better holds to higher k.

C. Bispectrum

We also compare the perturbative formula of the matter bispectrum at tree-level order (eqs. [20] and [36]) with the N-body results. Figure 6 shows the comparison of the reduced bispectrum Q between PT and N-body simulations at $z=0.3$ and 1:

$$Q(k_1, k_2, k_3) \equiv \frac{B(k_1, k_2, k_3)}{P(k_1)P(k_2) + P(k_2)P(k_3) + P(k_3)P(k_1)}. \tag{48}$$

We focus on the triangle configuration of $k_2/k_1 = 2$ varying the opening angle $\theta \equiv \arccos(\mathbf{k_1} \cdot \mathbf{k_2}/k_1/k_2)$ with different values of k_1 $[h$/Mpc$] = \{0.05, 0.1, 0.15, 0.2\}$. The overall amplitude of the reconstructed bispectrum decreases by reconstruction as R_s decreases. This is because the mode-coupling effect appeared in F_2 kernel is significantly reduced by reconstruction as shown in Figure 1. The reconstructed matter density field is thereby closer to be Gaussian. We find that the agreement between the tree-level PT and the N-body results is better after reconstruction as R_s is smaller upto $R_s = 8 - 10h^{-1}$Mpc. At smaller R_s, however, the nonlinearity in the smoothed density fields again cause the deviation of the bispectrum on small k as well as that of the power spectrum. The deviation should be improved by taking into account the one-loop components in the bispectrum [e.g., 13], however, we leave this work for the future.

D. Reconstruction using 2LPT

In this subsection, we show the reconstructed power spectrum using 2LPT instead of ZA. As shown in Figure 2, the negative amplitude due to the nonlinearity in the smoothing density field is alleviated by including the

2LPT correction term and the reconstructed spectrum is closer to the linear spectrum on small k. In order to confirm this, we use the N-body simulations to compute the reconstructed spectrum using 2LPT. We numerically compute the 2LPT correction term (eq. 39) by following the prescription written in Appendix D2 of [58]. In Fourier space, we compute the $\phi_{,ij}^{(1)}$ (i,j=1,2,3) terms by multiplying $\tilde{\delta}(k)$ by $-(k_ik_j/k^2)W(kR_s)$, transforming back to real space and computing the 2LPT source term in the right-hand side of eq. 39.

Figure 7 shows the comparison of PT with the N-body results when the matter density field is reconstructed using 2LPT. We confirm that the N-body results approach the linear spectrum for small k. This indicates that the nonlinearity in the smoothed density field can be partially canceled by using 2LPT. However, we find that the agreement with PT is not improved significantly by using 2LPT.

IV. SUMMARY AND CONCLUSIONS

We derive the one-loop order perturbative formula of the real-space matter power spectrum applied with the standard Lagrangian BAO reconstruction technique, in which the objects are displaced by the inverse ZA of the density field smoothed at R_s. We find that both of the next-leading one-loop terms P_{22} and P_{13} decrease in magnitude by reconstruction and thereby the reconstructed spectrum approaches the linear spectrum as long as the smoothed density field is close to linear, i.e, the smoothing scale $R_s \gtrsim 10h^{-1}$Mpc. Compared with N-body simulations, we find that our PT formula works also after reconstruction when the field is weakly non-Gaussian. When the smoothing scale R_s for the displacement field is smaller than $\sim 10h^{-1}$Mpc, however, we find deviations from the linear power spectrum on large scales (small k). By using the 2LPT approximation in reconstruction instead of inverse ZA, we find that this comes from the nonlinearity in the smoothed density field. Compared with the numerical simulations, we confirm that the numerical results show the behavior consistent with PT predictions in a wide range of R_s. We find that the agreement between PT and numerical simulations is better after reconstruction with $R_s \sim 8 - 10h^{-1}$Mpc. We also apply the RegPT to describe the nonlinearity in the reconstructed density field with the damping factor treated as a free parameter. We find that after reconstruction RegPT describes the matter power spectrum up to the third BAO peak ($k \sim 0.18h$/Mpc) at $z = 0.3$ and the fourth BAO peak ($k \sim 0.24h$/Mpc) at $z = 1$ even at one-loop order.

We also investigate the bispectrum for the reconstructed field in a perturbative manner. The amplitude of the bispectrum is found to decrease significantly after reconstruction. This is consistent with the fact that the nonlinear mode-coupling effect weakens by reconstruction and thereby the non-Gaussianity becomes smaller after reconstruction. We find that the tree-level PT
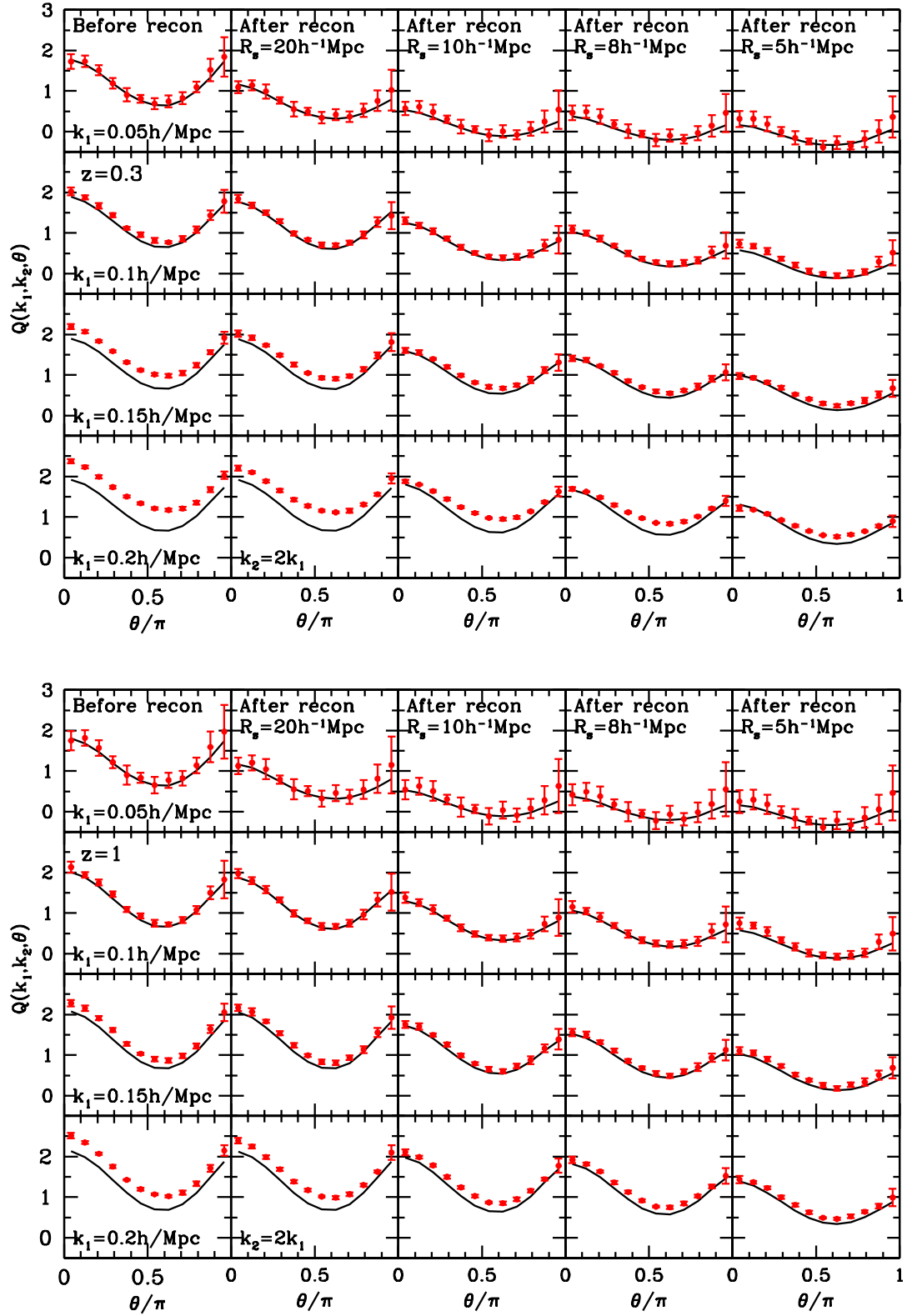
FIG. 6. Reduced bispectrum Q (eq. 48) for real-space dark matter field before and after ZA reconstruction with different smoothing scale $R_s = 20, 10, 8$ and $5h^{-1}$Mpc from left to right. The redshift is 0.3 (Upper) and 1 (Lower). The configuration of the triangle is fixed to be $k_2/k_1 = 2$ with $k_1 = 0.05, 0.1, 0.15, 0.2h$/Mpc (from top to bottom) and the opening angle $\theta \equiv \arccos(\mathbf{k_1} \cdot \mathbf{k_2}/k_1 k_2)$ is varied. Lines represent the tree-level PT (eqs. [20] and [36]) and the symbols are N-body results. The error-bars represent the 1σ dispersion of the N-body results with $1(h^{-1}\text{Gpc})^3$ volume.
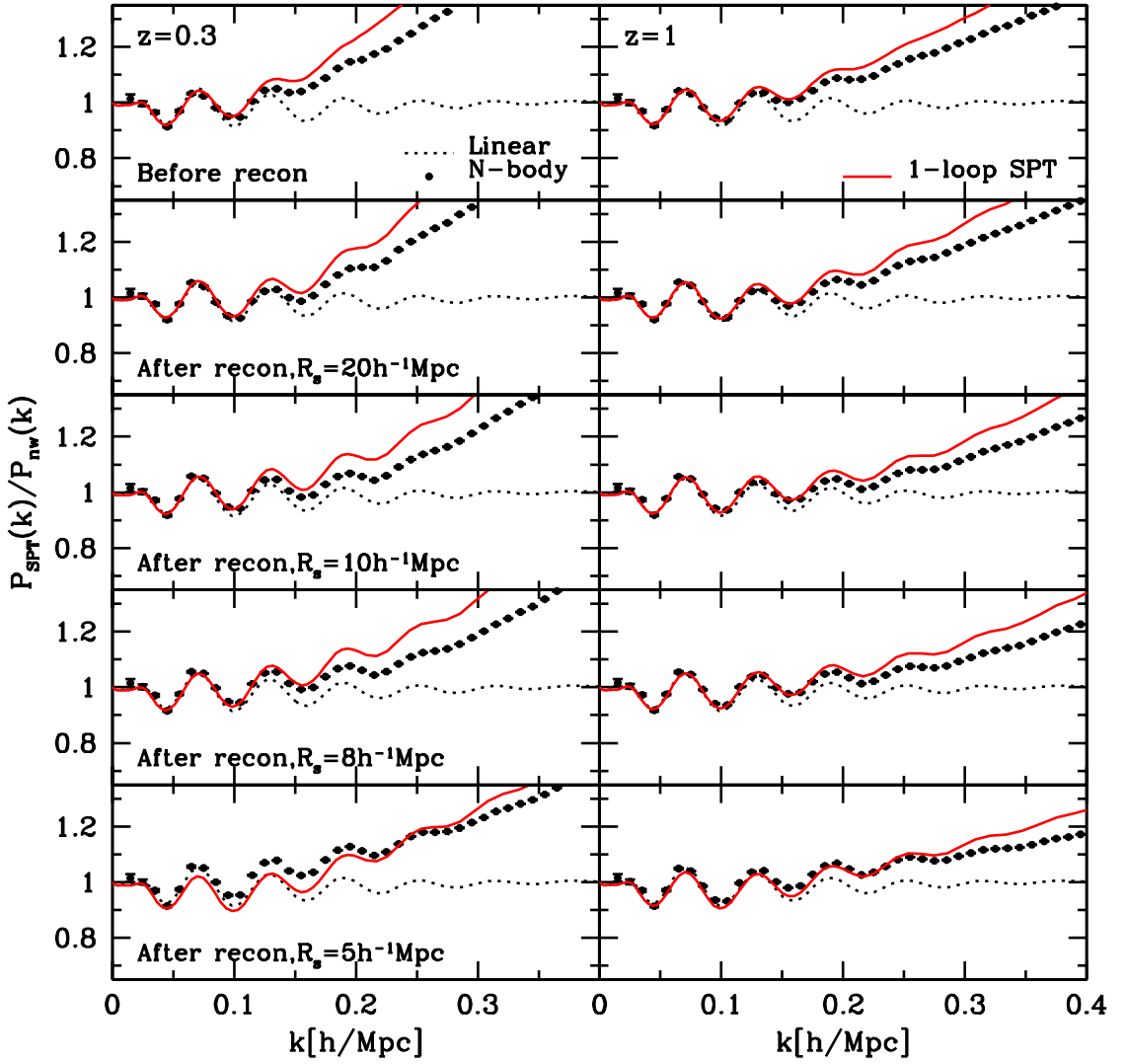
FIG. 7. Same as Fig. 3 but for the reconstructed power spectrum using 2LPT instead of ZA.

agrees with the simulation results in the weakly nonlinear regime, and the deviation between PT predictions and simulation results becomes smaller after reconstruction.

We confirm that the mode-coupling effect due to the nonlinear gravity becomes smaller by reconstruction in a perturbative approach. This may be practically useful to extract cosmological information from higher k modes than the previous work without reconstruction [e.g., 61, 62]. Two important caveats should be borne in mind: in order to apply our perturbative formula for the actual galaxy surveys, we have to take into account the other nonlinear effects such as redshift-space distortion and also galaxy bias. These nonlinear effects can also be incorporated in a perturbative manner [e.g., 11, 63–65].

Although there is evidence that galaxies are unbiased on large scales at low redshift [66], this is not true at high redshift (e.g. [67]), and it depends on the sample. We will present the application of our work to redshift-space clustering and also to the halo density fields in the next paper.

It is also interesting to study how the information of primordial density field is extracted from the reconstructed density field. Since the reconstructed field effectively approaches the initial density field, the reconstructed field is better suited to constrain the primordial information such as primordial non-Gaussianity [11, 13]. This is true unless the signature of the primordial information is not canceled by reconstruction.

Appendix A: Derivation of the Eulerian kernel for the reconstructed field

In this Appendix, we derive a perturbative formula of the reconstructed matter density field in real space. We expand the equation [29]) up to third order to derive the second- and third-order Eulerian kernels $F_n^{(\mathrm{rec})}(n = 2, 3)$. We take into account the higher-order terms of the shift field $\mathbf{s}(\mathbf{x})$ and the difference of Eulerian and Lagrangian positions in the shift field, $\mathbf{s}(\mathbf{x}) - \mathbf{s}(\mathbf{q})$.

1. $F_2^{(\mathrm{rec})}$ in ZA

As shown in equation (27), the leading order of the difference of the shift field evaluated at Eulerian and Lagrangian positions $\Delta \mathbf{s} = \mathbf{s}(\mathbf{x}) - \mathbf{s}(\mathbf{q})$ starts at second order:

$$\Delta \mathbf{s}^{(2)} = (\mathbf{\Psi}^{(1)} \cdot \nabla) \mathbf{s}^{(1)}, \tag{A1}$$

$$\Delta \mathbf{s}^{(3)} = (\mathbf{\Psi}^{(2)} \cdot \nabla) \mathbf{s}^{(1)} + (\mathbf{\Psi}^{(1)} \cdot \nabla) \mathbf{s}^{(2)}$$
$$+ \frac{1}{2} (\Psi_i^{(1)} \Psi_j^{(1)} \nabla_i \nabla_j) \mathbf{s}^{(1)}. \tag{A2}$$

The reconstructed density field given by equation (29) is rewritten as

$$\tilde{\delta}_{\mathbf{k}}^{(\mathrm{rec})} = \int \mathbf{dq} \, e^{-i\mathbf{k} \cdot \mathbf{q}} e^{-i\mathbf{k} \cdot \mathbf{s}(\mathbf{q})} (e^{-i\mathbf{k} \cdot [\mathbf{\Psi}(\mathbf{q}) + \Delta \mathbf{s}(\mathbf{q})]} - 1). \tag{A3}$$

The second order of $\tilde{\delta}_{\mathbf{k}}^{(\mathrm{rec})}$ is given by

$$\tilde{\delta}_{\mathbf{k}}^{(\mathrm{rec})(2)} = \int \mathbf{dq} \, e^{-i\mathbf{k} \cdot \mathbf{q}} \left[(-i\mathbf{k} \cdot \mathbf{\Psi}^{(2)}) + \frac{1}{2} (-i\mathbf{k} \cdot \mathbf{\Psi}^{(1)})^2 \right.$$
$$\left. + (-i\mathbf{k} \cdot \mathbf{s}^{(1)})(-i\mathbf{k} \cdot \mathbf{\Psi}^{(1)}) + (-i\mathbf{k} \cdot \Delta \mathbf{s}^{(2)}) \right]. \tag{A4}$$

The first two terms are included in the unreconstructed density field and their symmetrized kernels are respectively given as

$$F_2^{\Psi^{(2)}} = \frac{1}{2} \mathbf{k} \cdot \mathbf{L}^{(2)}(\mathbf{k}_1, \mathbf{k}_2), \tag{A5}$$

$$F_2^{\Psi^{(1)}, \Psi^{(1)}} = \frac{1}{2} (\mathbf{k} \cdot \mathbf{L}^{(1)}(\mathbf{k}_1))(\mathbf{k} \cdot \mathbf{L}^{(1)}(\mathbf{k}_2)). \tag{A6}$$

The last two terms come from the product of $\mathbf{\Psi}$ and $\mathbf{s}$, and the leading order of $\Delta \mathbf{s}$ as

$$F_2^{\mathbf{\Psi}^{(1)}, \mathbf{s}^{(1)}} = \frac{1}{2} [(\mathbf{k} \cdot \mathbf{S}^{(1)}(\mathbf{k}_1))(\mathbf{k} \cdot \mathbf{L}^{(1)}(\mathbf{k}_2)) + (1 \text{ perm.})], \tag{A7}$$

$$F_2^{\Delta \mathbf{s}^{(2)}} = -\frac{1}{2} [(\mathbf{k} \cdot \mathbf{S}^{(1)}(\mathbf{k}_1))(\mathbf{k}_1 \cdot \mathbf{L}^{(1)}(\mathbf{k}_2)) + (1 \text{ perm.})], \tag{A8}$$

where $\mathbf{S}^{(n)}$ is defined as the n-th kernel of the shift field $\mathbf{s}$ (eq. 24). The sum of the above two terms simplifies to

$$F_2^{\mathbf{\Psi}^{(1)}, \mathbf{s}^{(1)}} + F_2^{\Delta \mathbf{s}^{(2)}} = \frac{1}{2} [(\mathbf{k} \cdot \mathbf{S}^{(1)}(\mathbf{k}_1)) + (1 \text{ perm.})]. \tag{A9}$$

The $F_2^{(\mathrm{rec})}$ then is given by summing over all of the above components as

$$F_2^{(\mathrm{rec})}(\mathbf{k}_1, \mathbf{k}_2) = \frac{1}{2} \left[\mathbf{k} \cdot \mathbf{L}^{(2)}(\mathbf{k}_1, \mathbf{k}_2) \right.$$
$$+ (\mathbf{k} \cdot \mathbf{L}^{(1)}(\mathbf{k}_1))(\mathbf{k} \cdot \mathbf{L}^{(1)}(\mathbf{k}_2))$$
$$\left. + (\mathbf{k} \cdot \mathbf{S}^{(1)}(\mathbf{k}_1)) + (\mathbf{k} \cdot \mathbf{S}^{(1)}(\mathbf{k}_2)) \right] \tag{A10}$$
$$= \frac{5}{7} - \frac{W_1 + W_2}{2} + \frac{2}{7} \left(\frac{\mathbf{k}_1 \cdot \mathbf{k}_2}{k_1 k_2} \right)^2$$
$$+ \left(\frac{\mathbf{k}_1 \cdot \mathbf{k}_2}{2 k_1 k_2} \right) \left[\frac{k_2}{k_1} (1 - W_1) + \frac{k_1}{k_2} (1 - W_2) \right]. \tag{A11}$$

2. $F_3^{(\mathrm{rec})}$ in ZA

The third order of the reconstructed density fluctuation $\tilde{\delta}_{\mathbf{k}}^{(\mathrm{rec})}$ is given by

$$\tilde{\delta}_{\mathbf{k}}^{(\mathrm{rec})(3)} = \int \mathbf{dq} \, e^{-i\mathbf{k} \cdot \mathbf{q}} \left[(-i\mathbf{k} \cdot \mathbf{\Psi}^{(3)}) + (-i\mathbf{k} \cdot \mathbf{\Psi}^{(1)})(-i\mathbf{k} \cdot \mathbf{\Psi}^{(2)}) \right.$$
$$+ \frac{1}{6} (-i\mathbf{k} \cdot \mathbf{\Psi}^{(1)})^3 + (-i\mathbf{k} \cdot \mathbf{\Psi}^{(1)})(-i\mathbf{k} \cdot \Delta \mathbf{s}^{(2)})$$
$$+ (-i\mathbf{k} \cdot \Delta \mathbf{s}^{(3)}) + (-i\mathbf{k} \cdot \mathbf{s}^{(1)})$$
$$\times \left\{ (-i\mathbf{k} \cdot \mathbf{\Psi}^{(2)}) + \frac{1}{2} (-i\mathbf{k} \cdot \mathbf{\Psi}^{(1)})^2 + (-i\mathbf{k} \cdot \Delta \mathbf{s}^{(2)}) \right\}$$
$$+ (-i\mathbf{k} \cdot \mathbf{s}^{(2)})(-i\mathbf{k} \cdot \mathbf{\Psi}^{(1)})$$
$$\left. + \frac{1}{2} (-i\mathbf{k} \cdot \mathbf{s}^{(1)})^2 (-i\mathbf{k} \cdot \mathbf{\Psi}^{(1)}) \right], \tag{A12}$$

In the following, we derive the third-order kernel corresponding to each term including the factor associated with the perturbative expansion. All of the kernels are symmetrized among three wavevectors.

The first three terms are included in the unreconstructed density field and then each term is written as

follows:

$$F_3^{\mathbf{\Psi}^{(3)}} = \frac{1}{6}\mathbf{k}\cdot\mathbf{L}^{(3)}(\mathbf{k}_1,\mathbf{k}_2,\mathbf{k}_3), \tag{A13}$$

$$F_3^{\mathbf{\Psi}^{(1)},\mathbf{\Psi}^{(2)}} = \frac{1}{6}[(\mathbf{k}\cdot\mathbf{L}^{(1)}(\mathbf{k}_1))(\mathbf{k}\cdot\mathbf{L}^{(2)}(\mathbf{k}_2,\mathbf{k}_3))$$
$$+(2\text{ perms})], \tag{A14}$$

$$F_3^{\mathbf{\Psi}^{(1)},\mathbf{\Psi}^{(1)},\mathbf{\Psi}^{(1)}} = \frac{1}{6}(\mathbf{k}\cdot\mathbf{L}^{(1)}(\mathbf{k}_1))(\mathbf{k}\cdot\mathbf{L}^{(1)}(\mathbf{k}_2))(\mathbf{k}\cdot\mathbf{L}^{(1)}(\mathbf{k}_3)). \tag{A15}$$

The fourth term comes from the product of $\mathbf{\Psi}$ and $\Delta\mathbf{s}$

$$F_3^{\mathbf{\Psi}^{(1)},\Delta s^{(2)}} = -\frac{1}{6}\left[(\mathbf{k}\cdot\mathbf{S}^{(1)}(\mathbf{k}_1))(\mathbf{k}\cdot\mathbf{L}^{(1)}(\mathbf{k}_2))\right.$$
$$\left.\times(\mathbf{k}_1\cdot\mathbf{L}^{(1)}(\mathbf{k}_3)) + (5\text{ perms})\right]. \tag{A16}$$

The fifth term comes from $\Delta\mathbf{s}^{(3)}$ which has the three components given in equation (A2) and then the kernel corresponding to each component is given as follows:

$$F_3^{\mathbf{\Psi}^{(2)}\cdot\nabla\mathbf{s}^{(1)}} = -\frac{1}{6}[(\mathbf{k}\cdot\mathbf{S}^{(1)}(\mathbf{k}_1))(\mathbf{k}_1\cdot\mathbf{L}^{(2)}(\mathbf{k}_2,\mathbf{k}_3))$$
$$+(2\text{ perms})], \tag{A17}$$

$$F_3^{(\mathbf{\Psi}^{(1)}\cdot\nabla)\mathbf{s}^{(2)}} = -\frac{1}{6}[(\mathbf{k}\cdot\mathbf{S}^{(2)}(\mathbf{k}_1,\mathbf{k}_2))(\mathbf{k}_{12}\cdot\mathbf{L}^{(1)}(\mathbf{k}_3))$$
$$+(2\text{ perms})], \tag{A18}$$

$$F_3^{(\Psi_i^{(1)}\Psi_j^{(1)}\nabla_i\nabla_j)\mathbf{s}^{(1)}} = \frac{1}{6}[(\mathbf{k}\cdot\mathbf{S}^{(1)}(\mathbf{k}_1))(\mathbf{k}_1\cdot\mathbf{L}^{(1)}(\mathbf{k}_2))$$
$$\times(\mathbf{k}_1\cdot\mathbf{L}^{(1)}(\mathbf{k}_3)) + (2\text{ perms})]. \tag{A19}$$

The sixth and seventh terms come from the products of the first-order terms of $\mathbf{s}$ and the second-order terms of $\mathbf{\Psi}$:

$$F_3^{\mathbf{s}^{(1)},\mathbf{\Psi}^{(2)}} = \frac{1}{6}[(\mathbf{k}\cdot\mathbf{S}^{(1)}(\mathbf{k}_1))(\mathbf{k}\cdot\mathbf{L}^{(2)}(\mathbf{k}_2,\mathbf{k}_3))$$
$$+(2\text{ perms})], \tag{A20}$$

$$F_3^{\mathbf{s}^{(1)},\mathbf{\Psi}^{(1)},\mathbf{\Psi}^{(1)}} = \frac{1}{6}[(\mathbf{k}\cdot\mathbf{S}^{(1)}(\mathbf{k}_1))(\mathbf{k}\cdot\mathbf{L}^{(1)}(\mathbf{k}_2))$$
$$\times(\mathbf{k}\cdot\mathbf{L}^{(1)}(\mathbf{k}_3)) + (2\text{ perms})]. \tag{A21}$$

The eighth term is a combination of $\mathbf{s}$ and $\Delta\mathbf{s}$:

$$F_3^{\mathbf{s}^{(1)},\Delta\mathbf{s}^{(2)}} = -\frac{1}{6}[(\mathbf{k}\cdot\mathbf{S}^{(1)}(\mathbf{k}_1))(\mathbf{k}\cdot\mathbf{S}^{(1)}(\mathbf{k}_2))$$
$$\times(\mathbf{k}_{12}\cdot\mathbf{L}^{(1)}(\mathbf{k}_3)) + (2\text{ perms})]. \tag{A22}$$

The last two terms are the product of the second order of $\mathbf{s}$: and $\mathbf{\Psi}^{(1)}$

$$F_3^{\mathbf{\Psi}^{(1)},\mathbf{s}^{(2)}} = \frac{1}{6}[(\mathbf{k}\cdot\mathbf{S}^{(2)}((\mathbf{k}_1,\mathbf{k}_2))$$
$$\times(\mathbf{k}\cdot\mathbf{L}^{(1)}(\mathbf{k}_3)) + (2\text{ perms})], \tag{A23}$$

$$F_3^{\mathbf{\Psi}^{(1)},\mathbf{s}^{(1)},\mathbf{s}^{(1)}} = \frac{1}{6}[(\mathbf{k}\cdot\mathbf{S}^{(1)}(\mathbf{k}_1))(\mathbf{k}\cdot\mathbf{S}^{(1)}(\mathbf{k}_2))$$
$$\times(\mathbf{k}\cdot\mathbf{L}^{(1)}(\mathbf{k}_3)) + (2\text{ perms})]. \tag{A24}$$

Combinations of the above terms lead to some simplifications as follows:

$$F_3^{\mathbf{\Psi}^{(2)}\cdot\nabla\mathbf{s}^{(1)}} + F_3^{\mathbf{s}^{(1)},\mathbf{\Psi}^{(2)}} = \frac{1}{6}[(\mathbf{k}\cdot\mathbf{S}^{(1)}(\mathbf{k}_1))$$
$$\times(\mathbf{k}_{23}\cdot\mathbf{L}^{(2)}(\mathbf{k}_{23})) + (2\text{ perms})], \tag{A25}$$

$$F_3^{(\mathbf{\Psi}^{(1)}\cdot\nabla)\mathbf{s}^{(2)}} + F_3^{\mathbf{\Psi}^{(1)},\mathbf{s}^{(2)}} = \frac{1}{6}[\mathbf{k}\cdot\mathbf{S}^{(2)}(\mathbf{k}_1,\mathbf{k}_2)$$
$$+(2\text{ perms})], \tag{A26}$$

$$F_3^{\mathbf{s}^{(1)},\Delta\mathbf{s}^{(2)}} + F_3^{\mathbf{\Psi}^{(1)},\mathbf{s}^{(1)},\mathbf{s}^{(1)}} = \frac{1}{6}[(\mathbf{k}\cdot\mathbf{S}^{(1)}(\mathbf{k}_1))$$
$$\times(\mathbf{k}\cdot\mathbf{S}^{(1)}(\mathbf{k}_2)) + (2\text{ perms})], \tag{A27}$$

$$F_3^{\mathbf{s}^{(1)},\mathbf{\Psi}^{(1)},\mathbf{\Psi}^{(1)}} + F_3^{\mathbf{\Psi}^{(1)},\Delta s^{(2)}} + F_3^{(\Psi_i^{(1)}\Psi_j^{(1)}\nabla_i\nabla_j)\mathbf{s}^{(1)}}$$
$$= \frac{1}{6}[(\mathbf{k}\cdot\mathbf{S}^{(1)}(\mathbf{k}_1))(\mathbf{k}_{23}\cdot\mathbf{L}^{(1)}(\mathbf{k}_2))$$
$$\times(\mathbf{k}_{23}\cdot\mathbf{L}^{(1)}(\mathbf{k}_3)) + (2\text{ perms})]. \tag{A28}$$

The third-order kernel for the reconstructed density fields after reconstruction are then summarized as

$$F_3^{(\text{rec})}(\mathbf{k}_1,\mathbf{k}_2,\mathbf{k}_3) = F_3(\mathbf{k}_1,\mathbf{k}_2,\mathbf{k}_3)$$
$$+\frac{1}{6}\left[2(\mathbf{k}\cdot\mathbf{S}^{(1)}(\mathbf{k}_1))F_2(\mathbf{k}_2,\mathbf{k}_3)\right.$$
$$+(\mathbf{k}\cdot\mathbf{S}^{(1)}(\mathbf{k}_1))(\mathbf{k}\cdot\mathbf{S}^{(1)}(\mathbf{k}_2))$$
$$\left.+(\mathbf{k}\cdot\mathbf{S}^{(2)}(\mathbf{k}_1,\mathbf{k}_2)) + (2\text{ perms.})\right], \tag{A29}$$

where F_3 is the third-order kernel before reconstruction. The first term including the second-order Eulerian kernel comes from the sum of the equations (A25) and (A28).

When $(\mathbf{k}_1,\mathbf{k}_2,\mathbf{k}_3)=(\mathbf{k},\mathbf{p},-\mathbf{p})$, each component of the third-order kernel becomes

$$F_3^{\mathbf{\Psi}^{(2)}\cdot\nabla\mathbf{s}^{(1)}} + F_3^{\mathbf{s}^{(1)},\mathbf{\Psi}^{(2)}} = 0, \tag{A30}$$

$$F_3^{(\mathbf{\Psi}^{(1)}\cdot\nabla)\mathbf{s}^{(2)}} + F_3^{\mathbf{\Psi}^{(1)},\mathbf{s}^{(2)}} = -\frac{W(k_*)}{3}\left(\frac{1-r\mu}{1+r^2-2r\mu}\right)$$
$$\times\left(\frac{10r+4r\mu^2-7r^2\mu-7\mu}{7r}\right), \tag{A31}$$

$$F_3^{\mathbf{s}^{(1)},\Delta\mathbf{s}^{(2)}} + F_3^{\mathbf{\Psi}^{(1)},\mathbf{s}^{(1)},\mathbf{s}^{(1)}} = -\frac{W^2(kr)}{6}\frac{\mu^2}{r^2}, \tag{A32}$$

$$F_3^{\mathbf{s}^{(1)},\mathbf{\Psi}^{(1)},\mathbf{\Psi}^{(1)}} + F_3^{\mathbf{\Psi}^{(1)},\Delta s^{(2)}} + F_3^{(\Psi_i^{(1)}\Psi_j^{(1)}\nabla_i\nabla_j)\mathbf{s}^{(1)}}$$
$$= \frac{W(kr)}{3}\mu^2\left(1+\frac{1}{r^2}\right), \tag{A33}$$

where $r = p/k$, $\mu = \mathbf{k}\cdot\mathbf{p}/(kp)$ and $k_* \equiv k(1+r^2-2rx)^{1/2}$.

3. $F_3^{(\text{rec})}$ in 2LPT reconstruction

When reconstructing using 2LPT approximation instead of ZA, the second-order of the shift density field is

altered as

This corresponds to that the second-order kernel for the shift field in the 2LPT reconstruction as

$$\mathbf{S}^{(2)}(\mathbf{k}_1, \mathbf{k}_2) \rightarrow \mathbf{S}^{(2)}(\mathbf{k}_1, \mathbf{k}_2) + W_1 W_2 \mathbf{L}^{(2)}(\mathbf{k}_1, \mathbf{k}_2). \quad (A35)$$

When $(\mathbf{k}_1, \mathbf{k}_2, \mathbf{k}_3) = (\mathbf{k}, \mathbf{p}, -\mathbf{p})$, the equation (A31) becomes

$$
\begin{aligned}
F_3^{(\mathbf{\Psi}^{(1)} \cdot \nabla)\mathbf{s}^{(2)}} + F_3^{\mathbf{\Psi}^{(1)}, \mathbf{s}^{(2)}} = & -\frac{W(k_*)}{3} \left(\frac{1 - r\mu}{1 + r^2 - 2r\mu} \right) \\
& \times \left(\frac{10r + 4r\mu^2 - 7r^2\mu - 7\mu}{7r} \right) \\
& + W(k)W(kr)\frac{(1 - r\mu)(1 - \mu^2)}{7(1 + r^2 - 2r\mu)}. \quad (A36)
\end{aligned}
$$

$$
\begin{aligned}
\tilde{\mathbf{s}}^{(2)}_{\mathbf{k}} = & -iW(k)\mathbf{L}^{(1)}(\mathbf{k})\tilde{\delta}^{(2)}_{\mathbf{k}} + \frac{iD^2(z)}{2} \int \frac{d\mathbf{k}_1 d\mathbf{k}_2}{(2\pi)^3} \\
& \times \delta_{\mathrm{D}}(\mathbf{k}_1 + \mathbf{k}_2 - \mathbf{k}) W_1 W_2 \mathbf{L}^{(2)}(\mathbf{k}_1, \mathbf{k}_2)\tilde{\delta}^{(1)}_{\mathbf{k}_1}\tilde{\delta}^{(1)}_{\mathbf{k}_2}, \\
& \quad (A34)
\end{aligned}
$$

[1] D. J. Eisenstein, W. Hu, and M. Tegmark, ApJ **504**, L57 (1998), astro-ph/9805239.

[2] D. J. Eisenstein, I. Zehavi, D. W. Hogg, R. Scoccimarro, M. R. Blanton, R. C. Nichol, R. Scranton, H.-J. Seo, M. Tegmark, Z. Zheng, S. F. Anderson, J. Annis, N. Bahcall, J. Brinkmann, S. Burles, F. J. Castander, A. Connolly, I. Csabai, M. Doi, M. Fukugita, J. A. Frieman, K. Glazebrook, J. E. Gunn, J. S. Hendry, G. Hennessy, Z. Ivezić, S. Kent, G. R. Knapp, H. Lin, Y.-S. Loh, R. H. Lupton, B. Margon, T. A. McKay, A. Meiksin, J. A. Munn, A. Pope, M. W. Richmond, D. Schlegel, D. P. Schneider, K. Shimasaku, C. Stoughton, M. A. Strauss, M. SubbaRao, A. S. Szalay, I. Szapudi, D. L. Tucker, B. Yanny, and D. G. York, Astrophys. J. **633**, 560 (2005), astro-ph/0501171.

[3] S. Cole, W. J. Percival, J. A. Peacock, P. Norberg, C. M. Baugh, C. S. Frenk, I. Baldry, J. Bland-Hawthorn, T. Bridges, R. Cannon, M. Colless, C. Collins, W. Couch, N. J. G. Cross, G. Dalton, V. R. Eke, R. De Propris, S. P. Driver, G. Efstathiou, R. S. Ellis, K. Glazebrook, C. Jackson, A. Jenkins, O. Lahav, I. Lewis, S. Lumsden, S. Maddox, D. Madgwick, B. A. Peterson, W. Sutherland, and K. Taylor, MNRAS **362**, 505 (2005), astro-ph/0501174.

[4] N. Padmanabhan, D. J. Schlegel, U. Seljak, A. Makarov, N. A. Bahcall, M. R. Blanton, J. Brinkmann, D. J. Eisenstein, D. P. Finkbeiner, J. E. Gunn, D. W. Hogg, Ž. Ivezić, G. R. Knapp, J. Loveday, R. H. Lupton, R. C. Nichol, D. P. Schneider, M. A. Strauss, M. Tegmark, and D. G. York, MNRAS **378**, 852 (2007), astro-ph/0605302.

[5] W. J. Percival, R. C. Nichol, D. J. Eisenstein, J. A. Frieman, M. Fukugita, J. Loveday, A. C. Pope, D. P. Schneider, A. S. Szalay, M. Tegmark, M. S. Vogeley, D. H. Weinberg, I. Zehavi, N. A. Bahcall, J. Brinkmann, A. J. Connolly, and A. Meiksin, Astrophys. J. **657**, 645 (2007), astro-ph/0608636.

[6] T. Okumura, T. Matsubara, D. J. Eisenstein, I. Kayo, C. Hikage, A. S. Szalay, and D. P. Schneider, Astrophys. J. **676**, 889 (2008), arXiv:0711.3640.

[7] M. Tegmark, M. R. Blanton, M. A. Strauss, F. Hoyle, D. Schlegel, R. Scoccimarro, M. S. Vogeley, D. H. Weinberg, I. Zehavi, A. Berlind, T. Budavari, A. Connolly, D. J. Eisenstein, D. Finkbeiner, J. A. Frieman, J. E. Gunn, A. J. S. Hamilton, L. Hui, B. Jain, D. Johnston, S. Kent, H. Lin, R. Nakajima, R. C. Nichol, J. P. Ostriker, A. Pope, R. Scranton, U. Seljak, R. K. Sheth, A. Stebbins, A. S. Szalay, I. Szapudi, L. Verde, Y. Xu, J. Annis, N. A. Bahcall, J. Brinkmann, S. Burles, F. J. Castander, I. Csabai, J. Loveday, M. Doi, M. Fukugita, J. R. Gott, III, G. Hennessy, D. W. Hogg, Ž. Ivezić, G. R. Knapp, D. Q. Lamb, B. C. Lee, R. H. Lupton, T. A. McKay, P. Kunszt, J. A. Munn, L. O'Connell, J. Peoples, J. R. Pier, M. Richmond, C. Rockosi, D. P. Schneider, C. Stoughton, D. L. Tucker, D. E. Vanden Berk, B. Yanny, D. G. York, and SDSS Collaboration, Astrophys. J. **606**, 702 (2004), astro-ph/0310725.

[8] B. A. Reid, W. J. Percival, D. J. Eisenstein, L. Verde, D. N. Spergel, R. A. Skibba, N. A. Bahcall, T. Budavari, J. A. Frieman, M. Fukugita, J. R. Gott, J. E. Gunn, Z. Ivezic, G. R. Knapp, R. G. Kron, R. H. Lupton, T. A. McKay, A. Meiksin, R. C. Nichol, A. C. Pope, D. J. Schlegel, D. P. Schneider, C. Stoughton, M. A. Strauss, A. S. Szalay, M. Tegmark, M. S. Vogeley, D. H. Weinberg, D. G. York, and I. Zehavi, MNRAS **404**, 60 (2010), arXiv:0907.1659 [astro-ph.CO].

[9] M. Takada, E. Komatsu, and T. Futamase, Phys. Rev. D **73**, 083520 (2006), astro-ph/0512374.

[10] S. Saito, M. Takada, and A. Taruya, Phys. Rev. D **83**, 043529 (2011), arXiv:1006.4845 [astro-ph.CO].

[11] R. Scoccimarro, Phys. Rev. D **70**, 083007 (2004), astro-ph/0407214.

[12] A. Taruya, K. Koyama, and T. Matsubara, Phys. Rev. D **78**, 123534 (2008), arXiv:0808.4085.

[13] E. Sefusatti, Phys. Rev. D **80**, 123002 (2009), arXiv:0905.0717 [astro-ph.CO].

[14] V. Desjacques and U. Seljak, Advances in Astronomy **2010**, 908640 (2010), arXiv:1006.4763 [astro-ph.CO].

[15] A. Meiksin, M. White, and J. A. Peacock, MNRAS **304**, 851 (1999), astro-ph/9812214.

[16] V. Springel, S. D. M. White, A. Jenkins, C. S. Frenk, N. Yoshida, L. Gao, J. Navarro, R. Thacker, D. Croton, J. Helly, J. A. Peacock, S. Cole, P. Thomas, H. Couchman, A. Evrard, J. Colberg, and F. Pearce, Nature (London) **435**, 629 (2005), astro-ph/0504097.

[17] R. E. Angulo, C. M. Baugh, C. S. Frenk, R. G. Bower, A. Jenkins, and S. L. Morris, MNRAS **362**, L25 (2005),

astro-ph/0504456.

[18] H.-J. Seo and D. J. Eisenstein, Astrophys. J. **633**, 575 (2005), astro-ph/0507338.

[19] D. J. Eisenstein, H.-J. Seo, and M. White, Astrophys. J. **664**, 660 (2007), astro-ph/0604361.

[20] M. Crocce and R. Scoccimarro, Phys. Rev. D **77**, 023533 (2008), arXiv:0704.2783.

[21] M. Crocce and R. Scoccimarro, Phys. Rev. D **73**, 063519 (2006), astro-ph/0509418.

[22] T. Matsubara, Phys. Rev. D **77**, 063530 (2008), arXiv:0711.2521.

[23] A. Taruya, F. Bernardeau, T. Nishimichi, and S. Codis, Phys. Rev. D **86**, 103528 (2012), arXiv:1208.1191 [astro-ph.CO].

[24] J. J. M. Carrasco, M. P. Hertzberg, and L. Senatore, Journal of High Energy Physics **9**, 82 (2012), arXiv:1206.2926 [astro-ph.CO].

[25] D. J. Eisenstein, H.-J. Seo, E. Sirko, and D. N. Spergel, Astrophys. J. **664**, 675 (2007), astro-ph/0604362.

[26] N. Padmanabhan, M. White, and J. D. Cohn, Phys. Rev. D **79**, 063523 (2009), arXiv:0812.2905.

[27] H.-J. Seo, J. Eckel, D. J. Eisenstein, K. Mehta, M. Metchnik, N. Padmanabhan, P. Pinto, R. Takahashi, M. White, and X. Xu, Astrophys. J. **720**, 1650 (2010), arXiv:0910.5005 [astro-ph.CO].

[28] N. Padmanabhan, X. Xu, D. J. Eisenstein, R. Scalzo, A. J. Cuesta, K. T. Mehta, and E. Kazin, MNRAS **427**, 2132 (2012), arXiv:1202.0090.

[29] X. Xu, A. J. Cuesta, N. Padmanabhan, D. J. Eisenstein, and C. K. McBride, MNRAS **431**, 2834 (2013), arXiv:1206.6732.

[30] L. Anderson, É. Aubourg, S. Bailey, F. Beutler, V. Bhardwaj, M. Blanton, A. S. Bolton, J. Brinkmann, J. R. Brownstein, A. Burden, C.-H. Chuang, A. J. Cuesta, K. S. Dawson, D. J. Eisenstein, S. Escoffier, J. E. Gunn, H. Guo, S. Ho, K. Honscheid, C. Howlett, D. Kirkby, R. H. Lupton, M. Manera, C. Maraston, C. K. McBride, O. Mena, F. Montesano, R. C. Nichol, S. E. Nuza, M. D. Olmstead, N. Padmanabhan, N. Palanque-Delabrouille, J. Parejko, W. J. Percival, P. Petitjean, F. Prada, A. M. Price-Whelan, B. Reid, N. A. Roe, A. J. Ross, N. P. Ross, C. G. Sabiu, S. Saito, L. Samushia, A. G. Sánchez, D. J. Schlegel, D. P. Schneider, C. G. Scoccola, H.-J. Seo, R. A. Skibba, M. A. Strauss, M. E. C. Swanson, D. Thomas, J. L. Tinker, R. Tojeiro, M. V. Magaña, L. Verde, D. A. Wake, B. A. Weaver, D. H. Weinberg, M. White, X. Xu, C. Yèche, I. Zehavi, and G.-B. Zhao, MNRAS **441**, 24 (2014), arXiv:1312.4877.

[31] R. Tojeiro, A. J. Ross, A. Burden, L. Samushia, M. Manera, W. J. Percival, F. Beutler, J. Brinkmann, J. R. Brownstein, A. J. Cuesta, K. Dawson, D. J. Eisenstein, S. Ho, C. Howlett, C. K. McBride, F. Montesano, M. D. Olmstead, J. K. Parejko, B. Reid, A. G. Sánchez, D. J. Schlegel, D. P. Schneider, J. L. Tinker, M. V. Magaña, and M. White, MNRAS **440**, 2222 (2014), arXiv:1401.1768.

[32] E. A. Kazin, J. Koda, C. Blake, N. Padmanabhan, S. Brough, M. Colless, C. Contreras, W. Couch, S. Croom, D. J. Croton, T. M. Davis, M. J. Drinkwater, K. Forster, D. Gilbank, M. Gladders, K. Glazebrook, B. Jelliffe, R. J. Jurek, I.-h. Li, B. Madore, D. C. Martin, K. Pimbblet, G. B. Poole, M. Pracy, R. Sharp, E. Wisnioski, D. Woods, T. K. Wyder, and H. K. C. Yee, MNRAS **441**, 3524 (2014), arXiv:1401.0358.

[33] A. J. Ross, L. Samushia, C. Howlett, W. J. Percival, A. Burden, and M. Manera, MNRAS **449**, 835 (2015), arXiv:1409.3242.

[34] S. Alam, M. Ata, S. Bailey, F. Beutler, D. Bizyaev, J. A. Blazek, A. S. Bolton, J. R. Brownstein, A. Burden, C.-H. Chuang, J. Comparat, A. J. Cuesta, K. S. Dawson, D. J. Eisenstein, S. Escoffier, H. Gil-Marín, J. N. Grieb, N. Hand, S. Ho, K. Kinemuchi, D. Kirkby, F. Kitaura, E. Malanushenko, V. Malanushenko, C. Maraston, C. K. McBride, R. C. Nichol, M. D. Olmstead, D. Oravetz, N. Padmanabhan, N. Palanque-Delabrouille, K. Pan, M. Pellejero-Ibanez, W. J. Percival, P. Petitjean, F. Prada, A. M. Price-Whelan, B. A. Reid, S. A. Rodríguez-Torres, N. A. Roe, A. J. Ross, N. P. Ross, G. Rossi, J. A. Rubiño-Martín, A. G. Sánchez, S. Saito, S. Salazar-Albornoz, L. Samushia, S. Satpathy, C. G. Scóccola, D. J. Schlegel, D. P. Schneider, H.-J. Seo, A. Simmons, A. Slosar, M. A. Strauss, M. E. C. Swanson, D. Thomas, J. L. Tinker, R. Tojeiro, M. Vargas Magaña, J. A. Vazquez, L. Verde, D. A. Wake, Y. Wang, D. H. Weinberg, M. White, W. M. Wood-Vasey, C. Yèche, I. Zehavi, Z. Zhai, and G.-B. Zhao, ArXiv e-prints (2016), arXiv:1607.03155.

[35] M. Takada, R. Ellis, M. Chiba, J. E. Greene, H. Aihara, N. Arimoto, K. Bundy, J. Cohen, O. Doré, G. Graves, J. E. Gunn, T. Heckman, C. Hirata, P. Ho, J.-P. Kneib, O. Le Fèvre, L. Lin, S. More, H. Murayama, T. Nagao, M. Ouchi, M. Seiffert, J. Silverman, L. Sodré, Jr, D. N. Spergel, M. A. Strauss, H. Sugai, Y. Suto, H. Takami, and R. Wyse, ArXiv e-prints (2012), arXiv:1206.0737 [astro-ph.CO].

[36] DESI Collaboration, A. Aghamousa, J. Aguilar, S. Ahlen, S. Alam, L. E. Allen, C. Allende Prieto, J. Annis, S. Bailey, C. Balland, and et al., ArXiv e-prints (2016), arXiv:1611.00036 [astro-ph.IM].

[37] G. J. Hill, K. Gebhardt, E. Komatsu, N. Drory, P. J. MacQueen, J. Adams, G. A. Blanc, R. Koehler, M. Rafal, M. M. Roth, A. Kelz, C. Gronwall, R. Ciardullo, and D. P. Schneider, in *Panoramic Views of Galaxy Formation and Evolution*, Astronomical Society of the Pacific Conference Series, Vol. 399, edited by T. Kodama, T. Yamada, and K. Aoki (2008) p. 115, arXiv:0806.0183.

[38] L. Amendola, S. Appleby, A. Avgoustidis, D. Bacon, T. Baker, M. Baldi, N. Bartolo, A. Blanchard, C. Bonvin, S. Borgani, E. Branchini, C. Burrage, S. Camera, C. Carbone, L. Casarini, M. Cropper, C. de Rham, J. P. Dietrich, C. Di Porto, R. Durrer, A. Ealet, P. G. Ferreira, F. Finelli, J. Garcia-Bellido, T. Giannantonio, L. Guzzo, A. Heavens, L. Heisenberg, C. Heymans, H. Hoekstra, L. Hollenstein, R. Holmes, O. Horst, Z. Hwang, K. Jahnke, T. D. Kitching, T. Koivisto, M. Kunz, G. La Vacca, E. Linder, M. March, V. Marra, C. Martins, E. Majerotto, D. Markovic, D. Marsh, F. Marulli, R. Massey, Y. Mellier, F. Montanari, D. F. Mota, N. J. Nunes, W. Percival, V. Pettorino, C. Porciani, C. Quercellini, J. Read, M. Rinaldi, D. Sapone, I. Sawicki, R. Scaramella, C. Skordis, F. Simpson, A. Taylor, S. Thomas, R. Trotta, L. Verde, F. Vernizzi, A. Vollmer, Y. Wang, J. Weller, and T. Zlosnik, ArXiv e-prints (2016), arXiv:1606.00180.

[39] D. Spergel, N. Gehrels, C. Baltay, D. Bennett, J. Breckinridge, M. Donahue, A. Dressler, B. S. Gaudi, T. Greene, O. Guyon, C. Hirata, J. Kalirai, N. J. Kasdin, B. Macintosh, W. Moos, S. Perlmutter, M. Postman, B. Rauscher,

J. Rhodes, Y. Wang, D. Weinberg, D. Benford, M. Hudson, W.-S. Jeong, Y. Mellier, W. Traub, T. Yamada, P. Capak, J. Colbert, D. Masters, M. Penny, D. Savransky, D. Stern, N. Zimmerman, R. Barry, L. Bartusek, K. Carpenter, E. Cheng, D. Content, F. Dekens, R. Demers, K. Grady, C. Jackson, G. Kuan, J. Kruk, M. Melton, B. Nemati, B. Parvin, I. Poberezhskiy, C. Peddie, J. Ruffa, J. K. Wallace, A. Whipple, E. Wollack, and F. Zhao, ArXiv e-prints (2015), arXiv:1503.03757 [astro-ph.IM].

[40] E. T. Vishniac, MNRAS **203**, 345 (1983).

[41] J. N. Fry, Astrophys. J. **279**, 499 (1984).

[42] M. H. Goroff, B. Grinstein, S.-J. Rey, and M. B. Wise, Astrophys. J. **311**, 6 (1986).

[43] Y. Suto and M. Sasaki, Physical Review Letters **66**, 264 (1991).

[44] N. Makino, M. Sasaki, and Y. Suto, Phys. Rev. D **46**, 585 (1992).

[45] B. Jain and E. Bertschinger, Astrophys. J. **431**, 495 (1994), astro-ph/9311070.

[46] F. R. Bouchet, S. Colombi, E. Hivon, and R. Juszkiewicz, A.&Ap. **296**, 575 (1995), astro-ph/9406013.

[47] R. Scoccimarro and J. A. Frieman, Astrophys. J. **473**, 620 (1996), astro-ph/9602070.

[48] F. Bernardeau, S. Colombi, E. Gaztañaga, and R. Scoccimarro, Physics Report **367**, 1 (2002), astro-ph/0112551.

[49] D. Jeong and E. Komatsu, Astrophys. J. **651**, 619 (2006), astro-ph/0604075.

[50] P. Valageas, T. Nishimichi, and A. Taruya, Phys. Rev. D **87**, 083522 (2013), arXiv:1302.4533 [astro-ph.CO].

[51] Y. Noh, M. White, and N. Padmanabhan, Phys. Rev. D **80**, 123501 (2009), arXiv:0909.1802.

[52] M. Schmittfull, Y. Feng, F. Beutler, B. Sherwin, and M. Y. Chu, Phys. Rev. D **92**, 123522 (2015), arXiv:1508.06972.

[53] E. Komatsu, K. M. Smith, J. Dunkley, C. L. Bennett, B. Gold, G. Hinshaw, N. Jarosik, D. Larson, M. R. Nolta, L. Page, D. N. Spergel, M. Halpern, R. S. Hill, A. Kogut, M. Limon, S. S. Meyer, N. Odegard, G. S. Tucker, J. L. Weiland, E. Wollack, and E. L. Wright, ApJS **192**, 18 (2011), arXiv:1001.4538 [astro-ph.CO].

[54] P. Catelan, MNRAS **276**, 115 (1995), astro-ph/9406016.

[55] Y. B. Zel'dovich, A.&Ap. **5**, 84 (1970).

[56] B. D. Sherwin and M. Zaldarriaga, Phys. Rev. D **85**, 103523 (2012), arXiv:1202.3998 [astro-ph.CO].

[57] D. J. Eisenstein and W. Hu, Astrophys. J. **496**, 605 (1998), astro-ph/9709112.

[58] R. Scoccimarro, MNRAS **299**, 1097 (1998), astro-ph/9711187.

[59] M. Crocce, S. Pueblas, and R. Scoccimarro, MNRAS **373**, 369 (2006), astro-ph/0606505.

[60] F. Bernardeau, M. Crocce, and R. Scoccimarro, Phys. Rev. D **78**, 103521 (2008), arXiv:0806.2334.

[61] B. A. Reid, L. Samushia, M. White, W. J. Percival, M. Manera, N. Padmanabhan, A. J. Ross, A. G. Sánchez, S. Bailey, D. Bizyaev, A. S. Bolton, H. Brewington, J. Brinkmann, J. R. Brownstein, A. J. Cuesta, D. J. Eisenstein, J. E. Gunn, K. Honscheid, E. Malanushenko, V. Malanushenko, C. Maraston, C. K. McBride, D. Muna, R. C. Nichol, D. Oravetz, K. Pan, R. de Putter, N. A. Roe, N. P. Ross, D. J. Schlegel, D. P. Schneider, H.-J. Seo, A. Shelden, E. S. Sheldon, A. Simmons, R. A. Skibba, S. Snedden, M. E. C. Swanson, D. Thomas, J. Tinker, R. Tojeiro, L. Verde, D. A. Wake, B. A. Weaver, D. H. Weinberg, I. Zehavi, and G.-B. Zhao, MNRAS **426**, 2719 (2012), arXiv:1203.6641 [astro-ph.CO].

[62] F. Beutler, S. Saito, H.-J. Seo, J. Brinkmann, K. S. Dawson, D. J. Eisenstein, A. Font-Ribera, S. Ho, C. K. McBride, F. Montesano, W. J. Percival, A. J. Ross, N. P. Ross, L. Samushia, D. J. Schlegel, A. G. Sánchez, J. L. Tinker, and B. A. Weaver, ArXiv e-prints (2013), arXiv:1312.4611 [astro-ph.CO].

[63] A. F. Heavens, S. Matarrese, and L. Verde, MNRAS **301**, 797 (1998), astro-ph/9808016.

[64] T. Matsubara, Phys. Rev. D **78**, 083519 (2008), arXiv:0807.1733.

[65] A. Taruya, T. Nishimichi, and S. Saito, Phys. Rev. D **82**, 063522 (2010), arXiv:1006.0699.

[66] L. Verde, A. F. Heavens, W. J. Percival, S. Matarrese, C. M. Baugh, J. Bland-Hawthorn, T. Bridges, R. Cannon, S. Cole, M. Colless, C. Collins, W. Couch, G. Dalton, R. De Propris, S. P. Driver, G. Efstathiou, R. S. Ellis, C. S. Frenk, K. Glazebrook, C. Jackson, O. Lahav, I. Lewis, S. Lumsden, S. Maddox, D. Madgwick, P. Norberg, J. A. Peacock, B. A. Peterson, W. Sutherland, and K. Taylor, MNRAS **335**, 432 (2002), astro-ph/0112161.

[67] C.-T. Chiang, C. Wagner, A. G. Sánchez, F. Schmidt, and E. Komatsu, JCAP **9**, 028 (2015), arXiv:1504.03322.